Periodic Motions of Coupled Impact Oscillators

Guillaume James, Vincent Acary and Franck Pérignon

Abstract We study the existence and stability of time-periodic oscillations in a chain of coupled impact oscillators, for rigid impacts without energy dissipation. We formulate the search for periodic solutions as a boundary value problem incorporating unilateral constraints. This problem is solved analytically in the vicinity of the uncoupled limit and numerically for larger coupling constants. Different solution branches corresponding to nonlinear localized modes (breathers) and normal modes are computed.

1 Introduction

Understanding the dynamics of nonlinear lattices (i.e., large networks of coupled nonlinear oscillators) is a problem of fundamental importance in mechanics, condensed matter physics and biology. One of the major issues concerns the mathematical analysis and numerical computation of special classes of nonlinear time-periodic oscillation that organize the dynamics in many situations. In particular, spatially periodic waves (standing waves or periodic traveling waves) and spatially localized waves (breathers) are the object of intensive research [16, 41]. In this context, many

G. James (✉) · V. Acary · F. Pérignon
Université Grenoble Alpes, CNRS, Inria, Grenoble INP (Institute of Engineering, Université Grenoble Alpes), LJK, 38000 Grenoble, France
e-mail: guillaume.james@inria.fr

V. Acary
e-mail: vincent.acary@inria.fr

F. Pérignon
e-mail: franck.perignon@univ-grenoble-alpes.fr

R. I. Leine et al. (eds.), *Advanced Topics in Nonsmooth Dynamics*,
https://doi.org/10.1007/978-3-319-75972-2_3

theoretical and numerical works have focused on smooth nonlinear systems, whereas relatively few mathematical existence results are available for waves in nonsmooth infinite lattices [17, 18, 28, 39]. Developing theoretical and numerical tools for the analysis of nonlinear waves in nonsmooth systems is extremely important for applications, in particular, in the context of impact mechanics in which unilateral contacts and friction come into play [1, 5, 6, 15, 23]. Spatially discrete lattice models are frequently encountered in this context, in particular, for the modeling of waves in multibody mechanical systems (e.g., granular media) or in finite element models of continuum systems. A classical example illustrating the latter case concerns thin oscillating mechanical structures (a string under tension or a clamped beam) contacting rigid obstacles [5, 6, 23]. Such a structure can be described by a one-dimensional finite-element model involving a large number of degrees of freedom [2, 37]. The contact force between the string/beam and a rigid obstacle is either measure-valued (for rebounds with velocity jumps at contact times) or set-valued (if a wrapping of the string on the obstacle occurs) see, e.g., [13].

Although nonlinear modes of oscillation have been observed in experiments on impacting mechanical systems (see, e.g., [3, 6]), relatively little is known from a mathematical point of view about their existence and stability. Existence theorems for periodic and almost-periodic oscillations have been obtained in particular cases, for a continuum string model with point-mass or plane obstacle [9–11, 14, 20, 36] (see also [12] for a review). In addition, several analytical approaches have been used to obtain time-periodic solutions formally for different types of piecewise-linear dynamical systems with rigid impacts. One can mention Fourier and Green function methods [4–6, 17–19, 24–26, 33, 39], modal decomposition [29, 40] and sawtooth time transformations [34]. Most of the results obtained for discrete systems concern impacts localized on a *single particle*, and different types of wave have been constructed. In [29, 34, 40], nonsmooth normal modes have been obtained for general classes of conservative multiple degrees-of-freedom systems (the analysis in [34] is performed for a single or two impacting particles). Spatially-localized oscillations (breathers) with a single impacting node have also been studied for different classes of infinite or finite system. Breather existence and stability has been analyzed for oscillator chains with linear nearest-neighbor coupling and a symmetric local vibroimpact potential (including, in some cases, a linear component), both for conservative systems [18] and forced systems with dissipative impacts [17, 33, 39].

One of the main difficulties with the above techniques is the need to check analytically that the formal solutions to the piecewise-linear systems are consistent, i.e., that they satisfy the inequality constraints corresponding to non-penetration of the obstacles. This has been achieved in a number of works in the case of breathers [17, 18, 39] and for nonsmooth modes close to grazing linear normal modes [29]. In [19], the analysis from [33] has been extended to several impacting particles, but the verification of the inequality constraints is still an open problem in that case.

In this work, we study the existence and stability of time-periodic oscillations in an infinite chain of linearly coupled impact oscillators reminiscent of a model analyzed in [19, 33], for rigid impacts without energy dissipation. We show the existence of exact solutions (i.e., check the non-penetration conditions) for an arbitrary number of

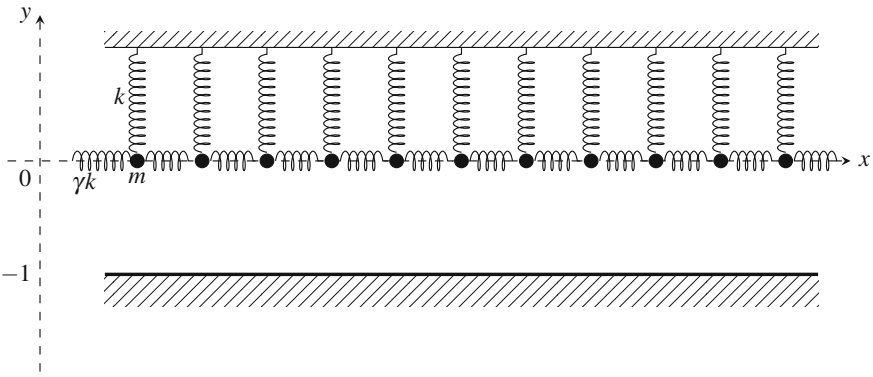

Fig. 1 A chain of identical impact oscillators with linear nearest-neighbor coupling. The chain is allowed to oscillate above a straight obstacle. After suitable rescaling, the obstacle position is fixed to $y = -1$, and the masses m of particles and local stiffness k are set to unity

impacting particles when the coupling between oscillators is small, and we compute solution branches numerically for larger couplings. The system under consideration is depicted in Fig. 1. Particle positions are denoted as $y(t) = (y_n(t))_{n\in\mathbb{Z}}$ and satisfy the following complementarity system:

$$\ddot{y}_n + y_n - \gamma\,(\Delta y)_n = \lambda_n, \quad n \in \mathbb{Z}, \tag{1}$$

$$0 \le \lambda \perp (y + \mathbb{1}) \ge 0, \tag{2}$$

$$\text{if } \dot{y}_n(t^-) < 0 \text{ and } y_n(t) = -1 \text{ then } \dot{y}_n(t^+) = -\dot{y}_n(t^-), \tag{3}$$

where $(\Delta y)_n = y_{n+1} - 2\,y_n + y_{n-1}$ defines a discrete Laplacian operator, $\mathbb{1}$ denotes the constant sequence with all terms equal to unity and $\gamma \ge 0$ is a parameter. Nondissipative impacts occur for $y_n(t) = -1$ and give rise to impulsive reaction forces $\lambda_n(t)$. This configuration differs from the case of a symmetric local vibroimpact potential considered in [19, 33], which introduces an additional barrier above the chain.

Our analytical results are presented in Sect. 2. We start by describing in Sect. 2.1 some simple examples of nonsmooth modes of oscillations (in-phase, out-of-phase, and some symmetry-breaking bifurcations from these modes). In Sect. 2.2, we reformulate the search for periodic solutions of (1)–(3) as a boundary value problem incorporating unilateral constraints. This formulation, together with an appropriate notion of nondegenerate modes introduced in Sect. 2.3, allows us to construct nonsmooth modes of oscillations (spatially localized or extended) at small coupling (see Theorems 1 and 2). This approach is an adaptation of the idea of an "anticontinuum" limit [16, 30, 38] to the nonsmooth setting. Section 2.4 deals with the linear stability of time-periodic solutions to (1)–(3). We provide a formula for the monodromy

matrix that determines spectral stability in the presence of simple impacts, following the lines of [32]. In Sect. 3, the above results are used for the numerical computation of time-periodic solutions. Solution branches are continued for fixed values of T, varying the linear stiffness γ (and starting from the limit $\gamma = 0$) or by fixing γ and varying T. In this way, we compute some families of breathers and extended modes and study their linear stability. Dynamical instabilities are illustrated by integrating (1)–(3) numerically. These computations are performed with the Siconos software for nonsmooth dynamical systems [1, 22].

2 Analytical Study of Nonsmooth Modes

2.1 Definitions and Basic Examples

We look for T-periodic solutions to (1)–(3) that are even in time, and assume each particle undergoes at most one impact during each period of oscillation. Consequently, for a given particle, impacts either occur at half-period multiples or do not occur at all. We denote by $I_k \subset \mathbb{Z}$ with $k = 1$ or 2 the index sets of particles impacting at $t = (2m + k)\,T/2$ for all $m \in \mathbb{Z}$ (i.e., $y_n((2m + k)\,T/2) = -1$), and by $I_0 := \mathbb{Z} \setminus (I_1 \cup I_2)$ the index set corresponding to non-impacting particles (i.e., $y_n(t) > -1$ for all t). We thus have $\lambda_n = 0$ for all $n \in I_0$ and

$$\lambda_n = 2\,\dot{y}_n\left(\frac{kT^+}{2}\right) \sum_{m\in\mathbb{Z}} \delta_{(m+\frac{k}{2})T} \quad \text{for all } n \in I_k. \tag{4}$$

The triplet (I_0, I_1, I_2) will be denoted as the *pattern* of the periodic solution. A *nonsmooth mode* corresponds to a continuous one-parameter family of periodic solutions (typically parameterized by T) sharing a given pattern with $I_0 \neq \mathbb{Z}$ (i.e., impacts occur).

We provide below some simple examples of nonsmooth modes. The simplest case corresponds to the in-phase mode with $I_1 = \mathbb{Z}$ (or equivalently, $I_2 = \mathbb{Z}$ up to a phase shift). This solution exists for $T \in (\pi, 2\pi)$ and reads as

$$y_n(t) = -\frac{\cos t}{\cos\,(T/2)} \text{ for } |t| \leq T/2, \tag{5}$$

where (5) is extended by periodicity outside the interval $(-T/2, T/2)$. The impact velocity in particular, reads as $\dot{y}_1((T/2)^+) = -\dot{y}_1((T/2)^-) = -\tan\,(T/2)$. The amplitude of oscillations diverges when $T \to \pi$ and becomes unity for $T = 2\pi$. In that case, the impact becomes grazing (i.e., occurs at zero velocity), and one recovers the *linear* in-phase mode $y_n(t) = \cos t$, which a solution to (1) with $\lambda = 0$. Notice that, for $T \neq 2\,k\,\pi$ outside the interval $(\pi, 2\pi)$, expression (5) does not provide a solution to (1)–(3), because the constraint $y_n \geq -1$ is violated.

Another example concerns nonsmooth modes with spatial period two, i.e., which satisfy $y_{n+2}(t) = y_n(t)$. Nonsmooth modes in two degrees-of-freedom impacting systems have been studied in a number of works (see, e.g., [31, 42] for a case of symmetric constraints and [23] for more references). In what follows, we discuss the case when I_1 and I_2 consist of the sets of odd and even integers, respectively. Moreover, we assume that all impact velocities are identical and nonzero. In order to compute such modes, we introduce the relative displacement $r = y_2 - y_1$, the center of mass $q = (y_1 + y_2)/2$ and the impact velocity $v = \dot{y}_2(0^+) = \dot{y}_1((T/2)^+) \neq 0$. From Eqs. (1) and (4) taken at $n = 1, 2$, and considering the spatial period two of the mode, one obtains

$$\ddot{r} + \Omega^2 r = 2\, v \sum_{m\in\mathbb{Z}} (-1)^m\, \delta_{m\,\frac{T}{2}}, \tag{6}$$

where $\Omega = \sqrt{1 + 4\,\gamma}$. Note that Ω is the frequency of the linear out-of-phase mode $y_n(t) = (-1)^n \cos(\Omega\, t)$, which is a solution to (1) with $\lambda = 0$. If the non-resonance condition $(2m + 1)\,(2\pi/T) \neq \Omega$ holds true for all integers m, there exists an even T-periodic solution to (6) defined by

$$r(t) = \frac{v}{\Omega}\, \frac{\sin(\Omega\,(t - \frac{T}{4}))}{\cos(\Omega\, T/4)} \text{ for } t \in [0, T/2], \tag{7}$$

where the integration constants have been determined from the conditions $v = \dot{r}(0^+) = \dot{r}((T/2)^-)$. In addition, the T-periodic solution is unique if $m\,(2\pi/T) \neq \Omega$ for all integers m. From expression (7), and using the fact that r is T-periodic and even, one can see that $r(\frac{T}{4} + t) = -r(\frac{T}{4} - t)$ for all $t \in \mathbb{R}$.

Similarly, the center of mass satisfies

$$\ddot{q} + q = v \sum_{m\in\mathbb{Z}} \delta_{m\,\frac{T}{2}}. \tag{8}$$

Let us assume that the non-resonance condition $T \neq 4\,m\,\pi$ holds true for all integers m. In that case, Eq. (8) admits an even $T/2$-periodic solution. Indeed, since $v/2 = \dot{q}(0^+) = -\dot{q}((T/2)^-)$, we find

$$q(t) = \frac{v}{2}\, \frac{\cos(t - \frac{T}{4})}{\sin(T/4)} \text{ for } t \in [0, T/2], \tag{9}$$

and q is defined as the $T/2$-periodic extension of (9). The symmetry $q(\frac{T}{4} + t) = q(\frac{T}{4} - t)$ for all $t \in \mathbb{R}$ and the fact that q is $T/2$-periodic imply that q is even. In addition, (8) does not possess additional T-periodic solutions if the non-resonance condition $T \neq 2\,m\,\pi$ holds true for all integers m.

Particle displacements are obtained from the identities

$$y_1 = q - \frac{r}{2}, \quad y_2 = q + \frac{r}{2}.$$

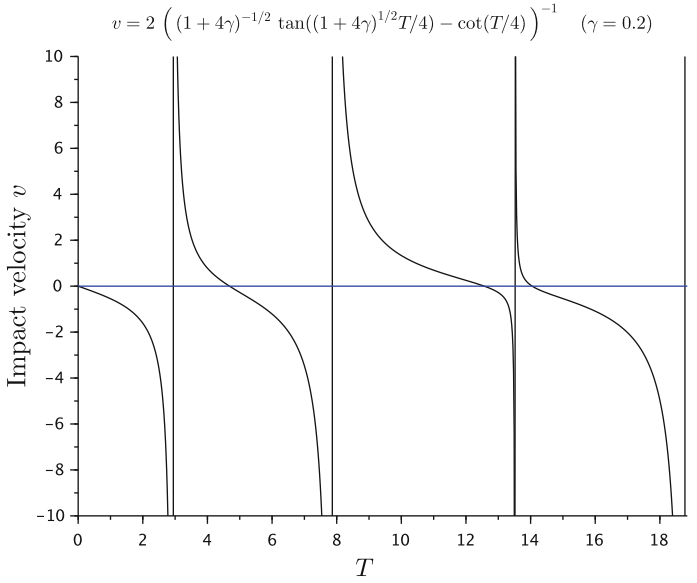

Fig. 2 Impact velocity as a function of the period

One can check that $\dot{y}_1(0^+) = 0$, hence $\dot{y}_1(0^-) = 0$ and y_1 is smooth everywhere except at the impact times $t = (2k+1)T/2$ with $k \in \mathbb{Z}$. Moreover, it follows from the symmetries of r that $y_2(t) = y_1(t + T/2) = y_1(t - T/2)$.

We use the constraint $y_2(0) = -1$ to determine v from T, which yields

$$v = 2\left(\frac{1}{\Omega}\tan(\Omega\, T/4) - \cot(T/4)\right)^{-1} \tag{10}$$

and implies that $y_1(T/2) = -1$. The expression in (10) is depicted in Fig. 2. In the uncoupled case $\gamma = 0$, expression (10) simplifies to $v = -\tan(T/2)$, and one recovers the case $n = 1$ of (5). Moreover, in the limit cases $T \to (2k+1)\,2\pi/\Omega$ ($k \in \mathbb{N}_0$) and $T \to 4m\pi$ ($m \in \mathbb{N}$), one obtains $v \to 0$, i.e., a grazing impact. When $T \to (2k+1)\,2\pi/\Omega$ and $\Omega \neq (2k+1)/(2m)$ for all $m \in \mathbb{N}$, the above solution converges towards the linear out-of-phase mode $y_n(t) = (-1)^{n+1}\cos(\Omega\, t)$, while $T \to 4m\pi$ and $\Omega \neq (2k+1)/(2m)$ for all $k \in \mathbb{N}_0$ leads to a convergence towards the linear in-phase mode $y_n(t) = -\cos t$.

In order to obtain solutions to (1)–(3), there remains to check the values of parameters γ, T for which the constraint $y_1 \geq -1$ is satisfied. Let us examine this problem when the coupling constant γ is fixed and T is varied. A necessary condition is $v \geq 0$, which is achieved for values of $T > 0$ within an infinite and unbounded sequence of disjoint intervals depending on γ. The lower bounds of these intervals are the roots of v^{-1}, and the upper bounds take the form $T = (2k+1)\,2\pi/\Omega$ with $k \in \mathbb{N}_0$ or $T = 4m\pi$ with $m \in \mathbb{N}$ (values leading to $v = 0$). In particular, the first interval

takes the form $(T_0(\gamma), 2\pi/\Omega]$, where $T_0(\gamma)$ is implicitely defined through

$$\frac{1}{\Omega}\tan(\Omega\, T_0/4) = \cot(T_0/4), \quad T_0 \in (0, 2\pi/\Omega). \tag{11}$$

Note that $\lim_{\gamma\to+\infty} T_0(\gamma) = 0$ (since $T_0 < 2\pi\,(1+4\gamma)^{-1/2}$), $\lim_{\gamma\to 0} T_0(\gamma) = \pi$ (the case $\Omega = 1$ of (11)), and T_0 is a decreasing function of γ (since the left side of (11) increases with Ω or γ), hence $T_0(\gamma) < \pi$ for $\gamma > 0$. The upper bound $T = 2\pi/\Omega$ yields $v = 0$ (grazing impact), as previously outlined, whereas in the case $T \to T_0(\gamma)^+$, one obtains $v \to +\infty$.

Now, let us check the constraint $y_1(t) \geq -1$ in the case $T \in (T_0(\gamma), 2\pi/\Omega)$. One can restrict the discussion to $t \in [0, T/2]$ without loss of generality (since y_1 is even and T-periodic). In that case, we deduce from the above computations that

$$\dot{y}_1(t) = -\frac{v}{2}\left(\frac{\sin(t-\frac{T}{4})}{\sin(T/4)} + \frac{\cos(\Omega\,(t-\frac{T}{4}))}{\cos(\Omega\,T/4)}\right).$$

Consequently, the conditions $T < 2\pi/\Omega < 2\pi$ and $v > 0$ (which follows from $T \in (T_0(\gamma), 2\pi/\Omega)$) imply that y_1 decreases on $[T/4, T/2]$, hence $y_1(t) > -1 = y_1(T/2)$ for all $t \in [T/4, T/2)$. In addition, expressions (7) and (9) show that $r \leq 0$ and $q > 0$ on $[0, T/4]$, hence $y_1 > 0$ on $[0, T/4]$. This shows that $y_1(t) > -1$ for all $t \in [0, T/2)$.

As a result, we have obtained a family of even and time-periodic solutions to (1)–(3), parameterized by their period $T \in (T_0(\gamma), 2\pi/\Omega)$. These solutions have spatial period two and possess the symmetry $y_{n+1}(t) = y_n(t + T/2)$. When $T \to T_0(\gamma)^+$, the impact velocity v and amplitude of oscillations $y_1(0)$ diverge. When $T \to 2\pi/\Omega$, the mode converges towards the linear out-of-phase mode. This family of solutions will be denoted as the *nonsmooth out-of-phase mode*. They are illustrated for several values of T in Fig. 3.

There exist other nonsmooth modes with spatial period 2 and $I_0 = \varnothing$, $I_2 = 2\,\mathbb{Z}$ not discussed above, for example, a branch of solutions emerging above $T = 4\pi/\Omega$. For $T = 4\pi/\Omega$, odd particles undergo a grazing impact at $t = 0$ (we conjecture the existence of a nonsmooth mode with two impacts per period and $T < 4\pi/\Omega$). When T increases above $4\pi/\Omega$, no impacts occur at $t = 0$ for odd particles and the branch of solutions can evolve in different ways depending on γ. If $\gamma < 5/16$ (so that $4\pi < 6\pi/\Omega$), the mode converges towards the linear in-phase mode when $T \to 4\pi^-$ (this corresponds to a period-doubling bifurcation of the in-phase mode), a limit in which odd particles again display a grazing impact at $t = 0$. If $\gamma > 5/16$ (the case $6\pi/\Omega < 4\pi$), convergence towards the linear out-of-phase mode takes place when $T \to (6\pi/\Omega)^-$ (period-tripling bifurcation of the out-of-phase mode). In this limit, odd particles undergo a grazing impact at $t = \pi/\Omega$. Illustrations of period doubling bifurcations are displayed in Fig. 4 and those period tripling bifurcations in Fig. 5.

Fig. 3 Nonsmooth out-of-phase modes for several values of T

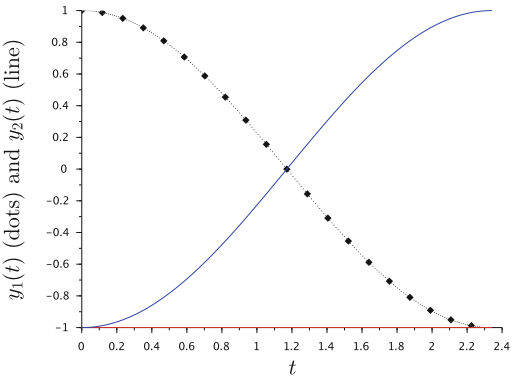

(a) Particle oscillations for $\gamma = 0.2, \quad T = 2\pi(1+4\gamma)^{-1/2} \approx 4.68$

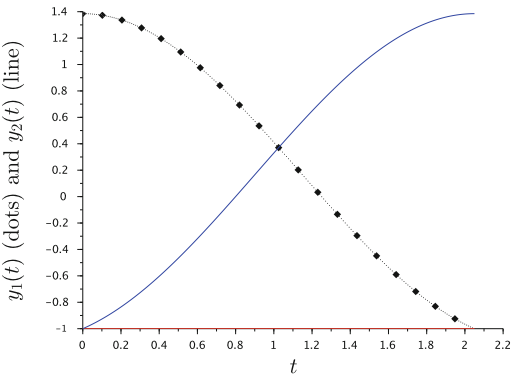

(b) Particle oscillations for $\gamma = 0.2, \quad T = 4.1$

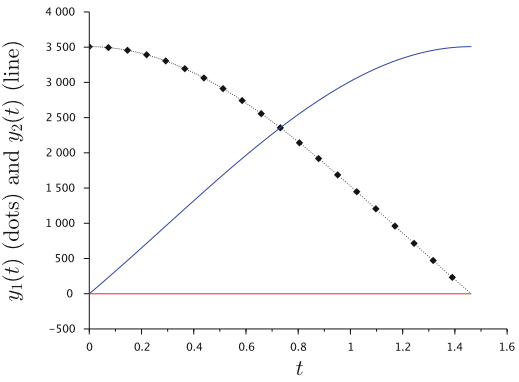

(c) Particle oscillations for $\gamma = 0.2, \quad T = 2.926$

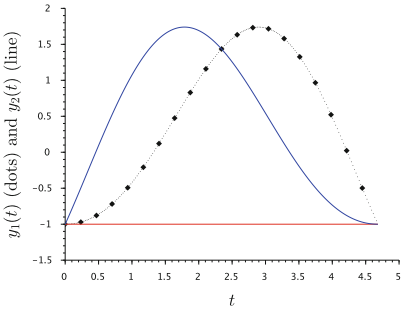

(a) Particle oscillations for $\gamma = 0.2, T = 4\pi(1 + 4\gamma)^{-1/2}$

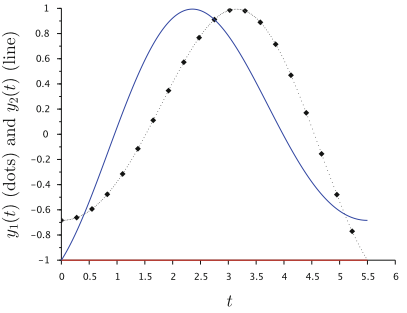

(b) Particle oscillations for $\gamma = 0.2, T = 11$

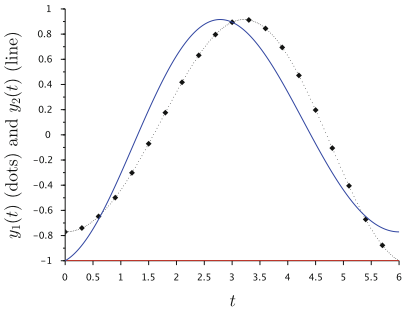

(c) Particle oscillations for $\gamma = 0.2, T = 12$

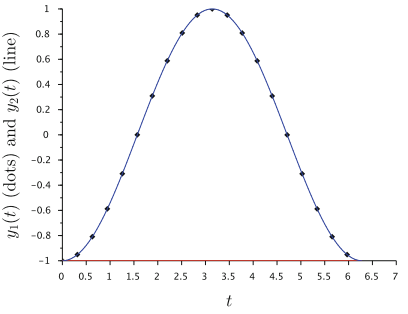

(d) Particle oscillations for $\gamma = 0.2, T = 4\pi$

Fig. 4 Period doubling bifurcation

2.2 Boundary Value Problem

In the sequel, E denotes either the Banach space $\ell_\infty(\mathbb{Z})$ of real bounded sequences on $\mathbb{Z}$, the Hilbert space $\ell_2(\mathbb{Z})$ of square-summable sequences, or the Hilbert space $\mathscr{P}^p$ of p-periodic sequences (isomorphic to the Euclidean space $\mathbb{R}^p$) for a fixed integer p. The case $E = \ell_2(\mathbb{Z})$ will be relevant for the study of localized modes, and the periodic case will be considered for numerical computations. We consider a chain of impact ocillators with positions described by a vector $y(t) \in E$ solution to the complementarity system (1)–(3). We look for T-periodic solutions even in time, with a prescribed pattern (I_0, I_1, I_2) (as defined in Sect. 2.1) such that $I_0 \neq \mathbb{Z}$.

The splitting $\mathbb{Z} = I_0 \cup I_1 \cup I_2$ allows one to identify E with $E^{(0)} \times E^{(1)} \times E^{(2)}$, where $E^{(k)}$ is a space of sequences indexed by $n \in I_k$, equiped with the same norm as E ($\|\ \|_2$ or $\|\ \|_\infty$). For all $y \in E$, we shall use the notation $y = (y^{(0)}, y^{(1)}, y^{(2)})$ with $y^{(k)} = (y_n)_{n \in I_k} \in E^{(k)}$. Any solution to the linear differential equation (12) satisfies $\dot{y}(t) \in E$, therefore we shall denote $\dot{y} = (\dot{y}^{(0)}, \dot{y}^{(1)}, \dot{y}^{(2)})$ with $\dot{y}^{(k)} \in E^{(k)}$. The above problem can be reformulated as a boundary value problem on a half-period interval $(0, T/2)$,

$$\ddot{y}_n + y_n - \gamma\,(\Delta y)_n = 0, \quad n \in \mathbb{Z}, \quad t \in (0, T/2), \tag{12}$$

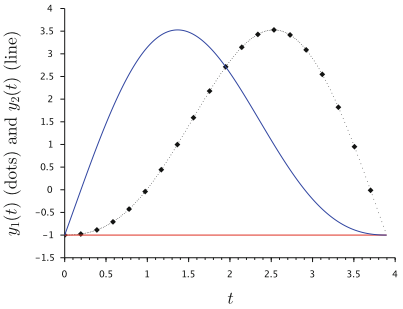

(a) Particle oscillations for $\gamma = 0.4, T = 4\pi(1 + 4\gamma)^{-1/2}$

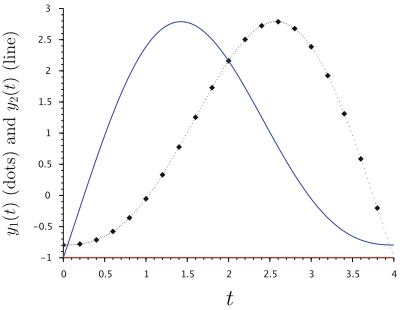

(b) Particle oscillations for $\gamma = 0.4, T = 8$

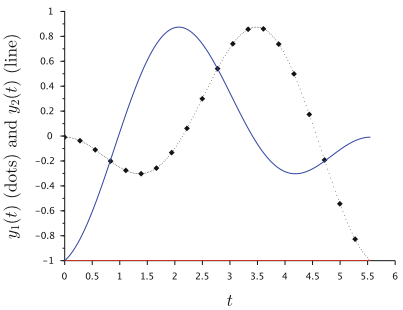

(c) Particle oscillations for $\gamma = 0.4, T = 11.1$

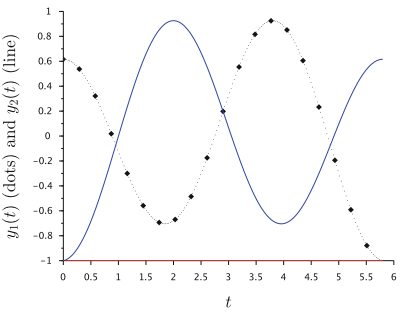

(d) Particle oscillations for $\gamma = 0.4, T = 11.6$

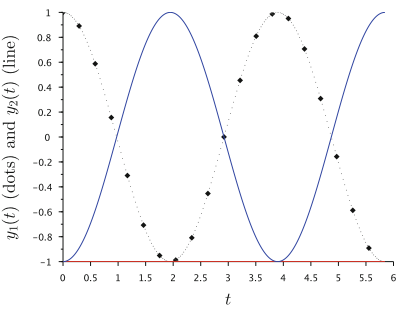

(e) Particle oscillations for $\gamma = 0.4, T = 6\pi(1 + 4\gamma)^{-1/2}$

Fig. 5 Period tripling bifurcation

with boundary conditions

$$\begin{aligned} \dot{y}^{(i)}(0) = 0 \text{ for } i \in I_0 \cup I_1 \ , \ y^{(2)}(0) = -\mathbb{1}, \\ \dot{y}^{(i)}(T/2) = 0 \text{ for } i \in I_0 \cup I_2 \ , \ y^{(1)}(T/2) = -\mathbb{1}, \end{aligned} \tag{13}$$

and constraint

$$y(t) + \mathbb{1} > 0, \quad t \in (0, T/2). \tag{14}$$

Indeed, it is immediately apparent that any even T-periodic solution to (1)–(3) with pattern (I_0, I_1, I_2) satisfies (12)–(14). Moreover, every solution to (12)–(14) can be extended to an even T-periodic function y, which, in turn, defines a solution to (1)–(3). Indeed, since $\dot{y}$ is odd, we have $\dot{y}(0^-) = -\dot{y}(0^+)$, and thus $\dot{y}((k\,T)^-) = -\dot{y}((k\,T)^+)$ for all $k \in \mathbb{Z}$ because $\dot{y}$ is T-periodic. In the same way, since $\dot{y}$ is odd and T-periodic, we have $\dot{y}((T/2)^-) = -\dot{y}((-T/2)^+) = -\dot{y}((T/2)^+)$, and thus we have, by periodicity, $\dot{y}(((2k+1)T/2)^-) = -\dot{y}(((2k+1)T/2)^+)$ for all $k \in \mathbb{Z}$.

In what follows, we reformulate the boundary value problem (12)–(13) as a linear system for $\xi = (y^{(0)}(0), y^{(1)}(0), \dot{y}^{(2)}(0)) \in E^{(0)} \times E^{(1)} \times E^{(2)}$, i.e., as an affine equation in E. For this purpose, we define the projection $P : E \times E \to E$ through

$$P\,(y, \dot{y}) = (\dot{y}^{(0)}, y^{(1)}, \dot{y}^{(2)})$$

and an embedding $N : E \to E \times E$ by

$$N\,(y^{(0)}, y^{(1)}, \dot{y}^{(2)}) = (u, v), \quad u = (y^{(0)}, y^{(1)}, 0), \ v = (0, 0, \dot{y}^{(2)}) \text{ in } E^{(0)} \times E^{(1)} \times E^{(2)}.$$

Introducing $Y = (y, \dot{y})^T \in E \times E$, the linear differential equation (12) takes the form

$$\dot{Y} = J\,Y + \gamma\,L\,Y, \tag{15}$$

where

$$J = \begin{pmatrix} 0 & \mathbb{I} \\ -\mathbb{I} & 0 \end{pmatrix}, \quad L = \begin{pmatrix} 0 & 0 \\ \Delta & 0 \end{pmatrix}$$

and $\mathbb{I}$ is the identity map in E. Let us denote by $S_\gamma(t) = e^{(J+\gamma L)\,t} \in \mathscr{L}(E \times E)$ the flow of (15).

The boundary condition at $t = 0$ defined in (13) takes the form $Y(0) = N\,\xi - B$, where $B = (\mathbb{1}_{I_2}, 0)^T \in E \times E$ and $\mathbb{1}_{I_2}$ denotes the indicator function of I_2. Moreover, the boundary condition at $t = T/2$ in (13) reads as $P\,Y(T/2) = -\mathbb{1}_{I_1}$. Consequently, the boundary value problem (12)–(13) is equivalent to

$$M_{\gamma,T}\,\xi = \eta, \tag{16}$$

where $M_{\gamma,T} = P\,S_\gamma(T/2)\,N \in \mathscr{L}(E)$ and $\eta = P\,S_\gamma(T/2)\,B - \mathbb{1}_{I_1}$.

In the case $E = \mathscr{P}^p$ (periodic boundary conditions with period p), E is isomorphic to $\mathbb{R}^p$ and (16) takes the form of a p-dimensional linear system. The solution $\xi \in E$ can be identified with a vector $x \in \mathbb{R}^p$ defined by

$$x_i = y_i \text{ if } i \in I_0 \cup I_1, \quad x_i = \dot{y}_i \text{ if } i \in I_2.$$

The matrix $P \in M_{p,2p}(\mathbb{R})$ reads as

$$P_{j,j} = 1 \text{ if } j \in I_1, \quad P_{j,j+p} = 1 \text{ if } j \in I_0 \cup I_2, \quad P_{i,j} = 0 \text{ elsewhere.}$$

The matrix $N \in M_{2p,p}(\mathbb{R})$ is defined by

$$N_{i,i} = 1 \text{ if } i \in I_0 \cup I_1, \quad N_{i+p,i} = 1 \text{ if } i \in I_2, \quad N_{i,j} = 0 \text{ elsewhere.}$$

2.3 Nondegenerate Modes and Continuation at Small Coupling

Consider an even T-periodic solution to (1)–(3) with pattern (I_0, I_1, I_2) (recall that under these assumptions, each particle undergoes at most one impact per period). The reduced initial condition $\xi = (y^{(0)}(0), y^{(1)}(0), \dot{y}^{(2)}(0)) \in E^{(0)} \times E^{(1)} \times E^{(2)}$ defines a solution to the linear problem (16). This leads us to introduce the following notion of a *nondegenerate* periodic solution.

Definition 1 An even T-periodic solution to (1)–(3) with pattern (I_0, I_1, I_2) is nondegenerate if the map $M_{\gamma,T}$ is invertible and

$$\dot{y}_n((T/2)^-) < 0 \,\forall n \in I_1, \quad \dot{y}_n(0^+) > 0 \,\forall n \in I_2. \tag{17}$$

Let us consider any nondegenerate periodic solution to (1)–(3). Since $M_{\gamma,T}$ depends analytically on γ, T, the corresponding solution to (16) *locally* admits a unique continuation with respect to (γ, T) denoted by $\xi_{\gamma,T}$, which is analytic in (γ, T) in some open set [43]. It follows that

$$Y_{\gamma,T}(t) = (y_{\gamma,T}(t), \dot{y}_{\gamma,T}(t))^T = S_\gamma(t)\,(N\,\xi_{\gamma,T} - B) \tag{18}$$

is a solution to (12) satisfying (13).

In order to check the constraint (14), we define $u_{\gamma,T}(t) = y_{\gamma,T}(\frac{T}{2}\,t) + \mathbb{1}$ and introduce the Banach space

$$X = \{\, u \in C^1([0,1], E), \quad u_n(1) = 0 \,\forall n \in I_1, \quad u_n(0) = 0 \,\forall n \in I_2 \,\},$$

equiped with the C^1-norm. We consider the *open* set

$$\begin{aligned}\Omega = \{\, & u \in X,\ \forall n \in I_0,\ u_n > 0 \text{ on } [0,1],\\ & \forall n \in I_1,\ u_n > 0 \text{ on } [0,1),\ \dot{u}_n(1^-) < 0,\\ & \forall n \in I_2,\ u_n > 0 \text{ on } (0,1],\ \dot{u}_n(0^+) > 0 \,\}.\end{aligned}$$

Thanks to assumption (17), the nondegenerate periodic solution belongs to Ω. Since the map $(\gamma, T) \mapsto u_{\gamma,T}$ is continuous in X, the local continuation with respect to (γ, T) of the nondegenerate solution stays locally in Ω, and thus the constraint (14) is satisfied by $y_{\gamma,T}$ when (γ, T) lies in some open set $\mathscr{U}$. Consequently, we have obtained a family of solutions to the boundary value problem (12)–(14) parameterized by (γ, T), which provides in turn a family of solutions to (1)–(3). As a result, we have shown the following.

Theorem 1 *Any nondegenerate even periodic solution to (1)–(3) with a given pattern persists for values of the coupling constant γ and period T lying in an open set $\mathscr{U}$. Moreover, these solutions take the form $y(t) = y_{\gamma,T}(t)$ for all $t \in [0, T/2]$, where the map $(t, \gamma, T) \mapsto y_{\gamma,T}(t)$ is analytic in $\mathbb{R} \times \mathscr{U}$ and defined in (18).*

In particular, the above result shows that any nondegenerate periodic solution is part of a continuous branch of periodic solutions parameterized by T and forming a nonsmooth mode. The continuation may stop when a new grazing impact takes place for $n \in I_0$ or if an impact occurring for $n \in I_1$ or I_2 becomes grazing. In such cases, the branch of periodic solutions might be continued with a different pattern or by allowing several impacts per period or sticking contacts, but these extensions are outside of the scope of the present study.

Another case when the above continuation theorem does not apply corresponds to the noninvertibility of $M_{\gamma,T}$. This situation may lead to a divergence of the solution (i.e., divergence of $\|(y^{(0)}(0), y^{(1)}(0), \dot{y}^{(2)}(0))\|$) or to a bifurcation of periodic solutions.

The solution to (12)–(13) is non-unique, or equivalently, $M_{\gamma,T}$ admits a nontrivial kernel if, and only if, the homogeneous boundary value problem given by (12) and

$$\begin{aligned}\dot{y}^{(i)}(0) = 0 \text{ for } i \in I_0 \cup I_1,\ y^{(2)}(0) = 0,\\ \dot{y}^{(i)}(T/2) = 0 \text{ for } i \in I_0 \cup I_2,\ y^{(1)}(T/2) = 0,\end{aligned} \tag{19}$$

admits nontrivial solutions $y(t) \in E$. Let us fix $E = \ell_\infty(\mathbb{Z})$ and discuss some *resonant* cases when this phenomenon occurs. The linear equation (12) admits normal mode solutions (or "phonons")

$$y_n(t) = a\, \cos(\Omega_q\, t + \varphi)\, \cos(q\, n + \psi), \tag{20}$$

whose frequencies $\Omega_q = (1 + 4\gamma\, \sin^2(q/2))^{1/2}$ span the phonon band $[1, \Omega]$, the highest frequency $\Omega = \sqrt{1 + 4\gamma}$ corresponding to the out-of-phase mode with $q = \pi$. For nonsmooth modes having certain patterns, simple nontrivial solutions to (12)–(19) can be found in the form (20) if some multiple of π/T belongs to the phonon band.

For example, if $I_1 = \mathbb{Z}$ or $I_2 = \mathbb{Z}$ (this is the case for the in-phase mode) and if one has a resonance $(2m+1)\,\pi/T = \Omega_q$ for some integer m and $q \in [0, \pi]$, then (20) provides nontrivial solutions to (12)–(19), and thus $M_{\gamma,T}$ is non-invertible. This occurs, e.g., for $T = \pi$ ($m = 0$, $q = 0$), where the amplitude of the in-phase mode becomes infinite.

Moreover, if one considers a localized pattern $I_0 = \mathbb{Z} \setminus \{n_0\}$ for some integer n_0, then the resonance $m\,(2\pi/T) = \Omega_q$ ($m \in \mathbb{N}$) leads to nontrivial solutions to (12)–(19) (obtained by choosing $\psi = \frac{\pi}{2} - q\,n_0$ in (20)), and thus $M_{\gamma,T}$ is non-invertible.

In the case $E = \mathscr{P}^p$ (p-periodic sequences), the phonon band becomes discrete (wavenumbers take the form $q = k\,2\pi/p$ with $k \in \mathbb{Z}$), but the above resonance conditions remain valid when $I_1 = \mathbb{Z}$ or $I_2 = \mathbb{Z}$, or if $I_0 = \mathbb{Z} \setminus \{n_0 + p\,\mathbb{Z}\}$.

As an application of Theorem 1, we now prove the existence of nonsmooth modes having any type of pattern, close to the uncoupled (or "anticontinuum") limit $\gamma = 0$. In Theorem 2 below, the mode pattern $I = (I_0, I_1, I_2)$ must be compatible with the choice of E. For $E = \mathscr{P}^p$, the sets I_k are assumed invariant modulo p, and for $E = \ell_2(\mathbb{Z})$, the sets I_1 and I_2 have to be finite (no impacts occur at infinity when oscillations are spatially localized). In the case $E = \ell_\infty(\mathbb{Z})$, there are no restrictions on the mode pattern.

Theorem 2 *Fix a mode pattern $I = (I_0, I_1, I_2)$ compatible with E. There exists an open set $\mathscr{V} \subset \mathbb{R}^2$ including the segment $\{0\} \times (\pi, 2\pi)$ such that for all $(\gamma, T) \in \mathscr{V}$, system (1)–(3) admits a unique even periodic solution with pattern I, which is defined by (18).*

Proof It suffices to check that for $\gamma = 0$ and all $T \in (\pi, 2\pi)$, system (1)–(3) admits a unique nondegenerate periodic solution with pattern I. Then, the result follows by direct application of Theorem 1.

Let us denote by $y_n^{\mathrm{ip}}(t)$ the in-phase mode defined by (5) with period $T \in (\pi, 2\pi)$. For $\gamma = 0$, system (1)–(3) consists of uncoupled impact oscillators. Consequently, the unique T-periodic solution with pattern I is given by $y_n = y_n^{\mathrm{ip}}$ for all $n \in I_1$, $y_n(t) = y_n^{\mathrm{ip}}(t + T/2)$ for all $n \in I_2$, and $y_n = 0$ for all $n \in I_0$ (for $\gamma = 0$, all non-impacting nontrivial solutions are 2π-periodic, and we have assumed that $T < 2\pi$). It follows that the condition (17) of non-grazing impacts is satistied for $T \in (\pi, 2\pi)$. In order to show that the T-periodic solution obtained for $\gamma = 0$ is nondegenerate, there remains to check that the linear map $M_{0,T}$ of (16) is invertible. We have, for all $\xi = (\xi^{(0)}, \xi^{(1)}, \xi^{(2)}) \in E^{(0)} \times E^{(1)} \times E^{(2)}$,

$$M_{0,T}\,\xi = P\,e^{J\,T/2} \begin{pmatrix} u \\ v \end{pmatrix}, \tag{21}$$

where $u, v \in E = E^{(0)} \times E^{(1)} \times E^{(2)}$ are defined as follows:

$$u = (\xi^{(0)}, \xi^{(1)}, 0), \quad v = (0, 0, \xi^{(2)}).$$

Moreover, we have in the block form

$$e^{J\,t} = \begin{pmatrix} \cos t & \sin t \\ -\sin t & \cos t \end{pmatrix} \in \mathscr{L}(E \times E),$$

hence (21) yields

$$M_{0,T}\,\xi = P\,(y, \dot{y}),$$

where $y, \dot{y} \in E = E^{(0)} \times E^{(1)} \times E^{(2)}$ are defined by

$$y = (\cos(T/2)\,\xi^{(0)}, \cos(T/2)\,\xi^{(1)}, \sin(T/2)\,\xi^{(2)}),$$

$$\dot{y} = (-\sin(T/2)\,\xi^{(0)}, -\sin(T/2)\,\xi^{(1)}, \cos(T/2)\,\xi^{(2)}).$$

Consequently, $M_{0,T} \in \mathscr{L}(E^{(0)} \times E^{(1)} \times E^{(2)})$ takes the following diagonal form:

$$M_{0,T}\,\xi = (-\sin(T/2)\,\xi^{(0)}, \cos(T/2)\,\xi^{(1)}, \cos(T/2)\,\xi^{(2)}).$$

It follows that $M_{0,T}$ is invertible because the coefficients $\cos(T/2)$ and $\sin(T/2)$ do not vanish for $T \in (\pi, 2\pi)$. □

It is interesting to compare the local continuation result of Theorem 2 and the explicit computations of the nonsmooth in-phase and out-of-phase modes performed in Sect. 2. The in-phase mode actually exists for all $\gamma \in \mathbb{R}$ and $T \in (\pi, 2\pi)$. Moreover, the out-of-phase mode exists for all $\gamma \geq 0$ (and even for γ slightly negative) and $T \in (T_0(\gamma), 2\pi(1+4\gamma)^{-1/2})$.

2.4 Stability

In this section, the linear stability of periodic solutions is analyzed through the eigenvalues of an associated monodromy matrix. Since the trajectory of the state of the system is nonsmooth at impact times, some precautions must be taken into account to compute the monodromy matrix. The computation of the monodromy follows the line of the work in [32].

In this section, we will consider the finite-dimensional case $E = \mathscr{P}^p$. For a given initial condition $Y_0 = (y(t_0), \dot{y}(t_0))^T \in \mathbb{R}^{2p}$, the conservative system (1)–(3) admits a unique solution (without accumulation of impacts) that is analytic in time between impacts [7, 8, 35]. Let us define the trajectory of the flow of (1)–(3) for the initial conditions (t_0, Y_0) as

$$\begin{array}{rcl} \phi : \mathbb{R} \times \mathbb{R} \times \mathbb{R}^{2p} & \to & \mathbb{R}^{2p} \\ (t, t_0, Y_0) & \mapsto & \phi(t, t_0, Y_0). \end{array} \tag{22}$$

The flow ϕ satisfies $\phi(t_0, t_0, Y_0) = Y_0$. The trajectory of the system for the initial condition (t_0, Y_0) is $Y(t) = \phi(t, t_0, Y_0)$. In the sequel, we consider a time t and

an initial time t_0 at which no impact occurs. The computation of the monodromy amounts to performing the differentiation of the flow ϕ at time t for the initial time t_0 with respect to the initial condition Y_0, that is,

$$M(t) = \frac{d\phi(t, t_0, Y_0)}{dY_0}. \tag{23}$$

This matrix can be approximated by finite differences. As noted in [32], the application of a finite-difference scheme may result in a poor approximation of the monodromy matrix. Since, in our application, the flow can be defined as a concatenation of piecewise smooth flows between impact times, we present here a closed-form formula for the monodromy matrix based on the computation of a saltation matrix that takes into account how the impact times evolve with the initial conditions. This closed-form formula is based on the assumption that the impacts are *simple impacts* in the sense that only one particle impacts at a given time. Moreover, we consider non-grazing impacts, i.e., impact at nonzero velocities.

The case of a simple impact at time $t_\star > t_0$:

Let us assume that we have a unique and simple impact in the interval (t_0, t) at time $t_\star(Y_0)$. The notation outlines its dependency on the initial condition. At the impact time $t_\star(Y_0)$, the trajectory is reset using the elastic Newton impact law, which can be written as follows:

$$Y(t_\star^+(Y_0)) = R_{t_\star} Y(t_\star^-(Y_0)), \tag{24}$$

where $R_{t_\star} \in \mathbb{R}^{2p\times 2p}$ is the reset matrix. Let us denote by $i_{t_\star}$ the index of the impacting particle at $t_\star(Y_0)$, i.e.,

$$y_{i_{t_\star}}(t_\star(Y_0)) = -1. \tag{25}$$

The reset matrix can be written as

$$R_{t_\star} = \begin{bmatrix} I & 0 \\ 0 & E \end{bmatrix}, \tag{26}$$

where the matrix $E \in \mathbb{R}^{p\times p}$ is given by its components as

$$E_{ij} = \begin{cases} 0, & \text{if } i \neq j, \\ 1, & \text{if } i = j \neq i_{t_\star}, \\ -1, & \text{if } i = j = i_{t_\star}. \end{cases} \tag{27}$$

The state of the system at time t can be written as

$$\begin{aligned} Y(t) &= \phi(t, t_0, Y_0) = \phi(t, t_\star^+(Y_0), Y(t_\star^+(Y_0))) \\ &= \phi(t, t_\star^+(Y_0), R_{t_\star} Y(t_\star^-(Y_0))) = \phi(t, t_\star^+(Y_0), R_{t_\star}\phi(t_\star^-(Y_0), t_0, Y_0)). \end{aligned} \tag{28}$$

The differentiation of the previous expression amounts to differentiating, with respect to Y_0, a composition of smooth functions

$$\begin{aligned}\frac{d\phi(t,t_0,Y_0)}{dY_0} &= D_2\phi(t,t_\star^+(Y_0),R_{t_\star}\phi(t_\star^-(Y_0),t_0,Y_0))\frac{dt_\star(Y_0)}{dY_0}\\ &\quad + D_3\phi(t,t_\star^+(Y_0),R_{t_\star}\phi(t_\star^-(Y_0),t_0,Y_0))R_{t_\star}\frac{d\phi(t_\star^-(Y_0),t_0,Y_0)}{dY_0}\end{aligned} \tag{29}$$

with

$$\frac{d\phi(t_\star^-(Y_0),t_0,Y_0)}{dY_0} = D_1\phi(t_\star^-(Y_0),t_0,Y_0)\frac{dt_\star(Y_0)}{dY_0} + D_3\phi(t_\star^-(Y_0),t_0,Y_0). \tag{30}$$

The notation $D_k\phi$ denotes the partial derivatives of ϕ with respect to its k-th argument. If the smooth flow is known between impacts, the only difficult part that remains to compute is the derivative of the time of impact $t_\star$ with respect to Y_0. Let us split the flow ϕ such that

$$Y(t) = \phi(t,t_0,Y_0) = \begin{bmatrix}\phi_y(t,t_0,Y_0)\\ \phi_{\dot y}(t,t_0,Y_0)\end{bmatrix} = \begin{bmatrix}y(t)\\ \dot y(t)\end{bmatrix}. \tag{31}$$

We have assumed that only one particle of index $i_{t_\star}$ is impacting at $t_\star(Y_0)$. The constraint (25) can be written as

$$\phi_{y,i_{t_\star}}(t_\star,t_0,Y_0) = -1. \tag{32}$$

Since $\partial_t\phi_{y,i_{t_\star}}(t_\star^-,t_0,Y_0) = \dot y_{i_{t_\star}}(t_\star^-(Y_0)) < 0$ (non-grazing impact) and the flow is smooth (analytic) between impacts, the implicit function theorem guarantees that the impact persists upon small variations of Y_0, with an impact time $t_\star$ being a smooth (analytic) function of Y_0. Moreover, defining a projection matrix $P_i \in \mathbb{R}^{1\times 2p}$ such that

$$D_3\phi_{y,i}(t_\star^-(Y_0),t_0,Y_0) = P_i D_3\phi(t_\star^-(Y_0),t_0,Y_0), \tag{33}$$

we have

$$\frac{dt_{t_\star}(Y_0)}{dY_0} = -\frac{1}{\dot y_{i_{t_\star}}(t_\star^-(Y_0))}P_{i_{t_\star}}D_3\phi(t_\star^-(Y_0),t_0,Y_0). \tag{34}$$

In order to simplify the expression of the monodromy matrix given by (29) and (30), we observe that

$$D_2\phi(t,t_\star^+,Y(t_\star^+(Y_0))) = -D_3\phi(t,t_\star^+(Y_0),Y(t_\star^+(Y_0)))\dot Y(t_\star^+(Y_0)). \tag{35}$$

Indeed, since $\phi(t,\tilde t,\phi(\tilde t,t_\star^+,Y_\star)) = \phi(t,t_\star^+,Y_\star)$ is independent of $\tilde t$, the identity $\partial_{\tilde t}\phi(t,\tilde t,\phi(\tilde t,t_\star^+,Y_\star)) = 0$ evaluated at $\tilde t = t_\star^+$ and $Y_\star = Y(t_\star^+(Y_0))$ yields identity (35). Using (29), (30) and (35), the monodromy matrix simplifies to

$$\frac{d\phi(t,t_0,Y_0)}{dY_0} = D_3\phi(t,t_\star^+,Y(t_\star^+(Y_0))) \left[[R_{t_\star}\dot{Y}(t_\star^-(Y_0)) - \dot{Y}(t_\star^+(Y_0))]\frac{dt_\star(Y_0)}{dY_0} + R_{t_\star}D_3\phi(t_\star^-(Y_0),t_0,Y_0)\right]. \tag{36}$$

Finally, using the relation (34), the monodromy matrix is expressed as follows:

$$\frac{d\phi(t,t_0,Y_0)}{dY_0} = D_3\phi(t,t_\star^+(Y_0),Y(t_\star^+(Y_0)))S_{t_\star}D_3\phi(t_\star^-(Y_0),t_0,Y_0), \quad t > t_\star(Y_0), \tag{37}$$

where the so-called saltation matrix $S_{t_\star}$ is defined by

$$S_{t_\star} = -\frac{1}{\dot{y}_{i_{t_\star}}(t_\star^-(Y_0))}[R_{t_\star}\dot{Y}(t_\star^-(Y_0)) - \dot{Y}(t_\star^+(Y_0))]P_{i_{t_\star}} + R_{t_\star}. \tag{38}$$

Note that the monodromy matrix is obtained as the product of the Jacobian matrices of the flow with respect to the initial condition in each smooth phase separated by the saltation matrix.

The Case of Two Simple Impacts at Times $t_{\star,2} > t_{\star,1} > t_0$:

For the two simple impacts at time $t_{\star,2} > t_{\star,1} > t_0$, the computation of the monodromy matrix follows the same line. It is also a product of the Jacobian matrices of the flow with respect to the initial condition in each smooth phase separated by the saltation matrix:

$$\frac{d\phi(t,t_0,Y_0)}{dY_0} = D_3\phi(t,t_{\star,2}^+(Y_0),Y(t_{\star,2}^+(Y_0)))S_{t_{\star,2}} D_3\phi(t,t_{\star,1}^+(Y_0),Y(t_{\star,1}^+(Y_0)))S_{t_{\star,1}}D_3\phi(t_{\star,1}^-(Y_0),t_0,Y_0), \quad t > t_{\star,2}(Y_0). \tag{39}$$

Computation of the Monodromy for the Piecewise Linear System :

In our case of a piecewise-linear dynamics, the flow of the system between two impacts is given by

$$\phi(t,t_0,Y_0) = \exp(D(t-t_0))\,Y_0,\ t_0 \le t \le t_{\star,1}(Y_0), \tag{40}$$

$$\phi(t,t_{\star,1}^+(Y_0),Y(t_{\star,1}^+(Y_0))) = \exp(D(t-t_{\star,1}(Y_0)))\,Y(t_{\star,1}^+(Y_0)),\ t_{\star,1}(Y_0) \le t \le t_{\star,2}(Y_0) \tag{41}$$

$$\phi(t,t_{\star,2}^+(Y_0),Y(t_{\star,2}^+(Y_0))) = \exp(D(t-t_{\star,2}(Y_0)))\,Y(t_{\star,2}^+(Y_0)),\ t \ge t_{\star,2}(Y_0), \tag{42}$$

with $D = J + \gamma L$. As indicated above in the derivation of the monodromy matrix, the piecewise linear flow is smooth (analytic). If we consider the explicit formula of the linear flow (40)–(42) between impacting times at $t_{\star,1} = T/2$ and $t_{\star,2} = T$, we get, for the monodromy matrix,

$$\frac{d\phi(t, t_0, Y_0)}{dY_0} = \exp(D(t-T))\, S_T\, \exp(D(T/2))\, S_{T/2}\, \exp(D(T/2-t_0)), \quad t > T, \tag{43}$$

where $t_0 < T/2$. In Sect. 3, we shall fix $t_0 = T/4$ and $t = t_0 + T = 5T/4$ to compute the monodromy matrix of a T-periodic solution with impact times multiple of $T/2$. This leads to

$$\frac{d\phi(5T/4, T/4, Y_0)}{dY_0} = \exp(DT/4)\, S_T\, \exp(D(T/2))\, S_{T/2}\, \exp(DT/4). \tag{44}$$

The periodic solution will be unstable if this monodromy matrix admits an eigenvalue with modulus greater than unity, and spectrally stable if all eigenvalues lie on the unit circle (due to time-reversal symmetry, the Floquet spectrum has the invariance $\sigma \to \sigma^{-1}$). The spectrum of the above monodromy is the same as for $S_T\, \exp(D(T/2))\, S_{T/2}\, \exp(DT/2)$.

3 Numerical Computation of Nonsmooth Modes

We solve problem (12)–(13) numerically for a chain of p oscillators with periodic boundary conditions. Unless explicitly stated otherwise, we fix $p = 100$. Although the system (12)–(13) is a standard linear system, we use a general shooting method, i.e., determine a vector $\xi = (y^{(0)}(0), y^{(1)}(0), \dot{y}^{(2)}(0)) \in \mathbb{R}^p$ such that the three boundary conditions of (13) at $t = 0$ and $t = T/2$ are satisfied through Newton iterations. For each Newton iteration, this requires solving a linear system for ξ obtained through time-integration of the linear ODE (12). This time integration is equivalent to computing the exponential matrix of the linear flow numerically. When the coupling parameter is chosen far from the degeneracy case of the BVP matrix, the shooting technique converges in one iteration. When we are in the neighborhood of the degenerate cases, the number of Newton iterations may increase, indicating an ill-conditioned linear system of the BVP. Thanks to the general shooting technique, the case of nonlinear local or interaction potentials could be similarly addressed. The constraint (14) is checked *a posteriori*. To this end, we integrate (1)–(3) numerically using an event-driven scheme for nonsmooth dynamical systems implemented in the Siconos software [22]. For the shooting technique and validation of the constraints, the linear ODE is integrated thanks to ODEPACK [21] embedded in the Siconos software.

Usually, the solution branches are first continued for fixed values of T, varying the coupling parameter γ. For all fixed value $T \in (\pi, 2\pi)$, a choice of impacting particles and phases (determined by I_1, I_2) selects a unique solution for $\gamma = 0$, which can be continued up to some maximal value of the coupling parameter γ. We shall see in the sequel that some continuations are also done with respect to the period.

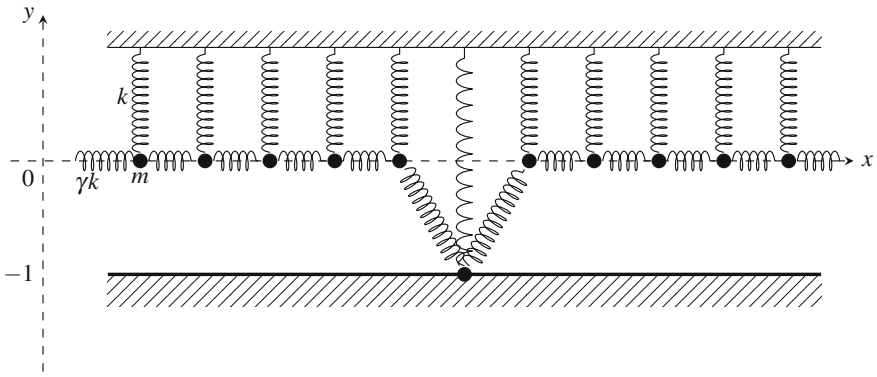

Fig. 6 Mode pattern for the site-centered breather

3.1 Site-Centered Breathers

In this section, we illustrate the site-centered breather for the mode pattern $I_2 = \{50\}$, $I_1 = \emptyset$ depicted in Fig. 6. The period is $T = \frac{3\pi}{2}$. The periodic solution has been successfully computed for $\gamma \in [0, \gamma_c]$ with

$$\gamma_c = \frac{1}{4}\left(\left(\frac{2\pi}{T}\right)^2 - 1\right), \tag{45}$$

the critical value of γ for which we expect to reach the out-of-phase mode. For $T = \frac{3\pi}{2}$, we have $\gamma_c \approx 0.1944$. In Fig. 7, the initial positions and velocities are displayed for the particle indices between 40 and 60 and for 4 different values of γ. We observe that, for small values of the coupling parameter γ, the breather is localized on a few particles. With the increasing values of γ, the support of the solution is increasing to reach the out-of-phase linear grazing mode for $\gamma = \gamma_c$. Let us note that the velocity of the central particle 50 is decreasing to the grazing solution for all the particles.

In Fig. 8, the eigenvalues of the monodromy matrix are displayed. In Fig. 8a, we remark that the eigenvalues have a modulus equal to 1 up to a critical value γ_s between 0.129 and 0.142 for which a pair of eigenvalues is leaving the unit circle. In Fig. 8b, c and d, all the eigenvalues are plotted in the complex plane for three different values of $\gamma \in \{0, 0.064, 0.181\}$. For $\gamma = 0$, a pair of eigenvalues are equal to $+1$ and all the other conjugate eigenvalues pairs are equal to i or $-i$. For $\gamma < \gamma_s$, the conjugate eigenvalue pairs, equal to i and $-i$ for $\gamma = 0$, start to slide on the unit circle toward the pair of eigenvalues that remains at $+1$. For $\gamma = \gamma_s$, a collision occurs at $+1$. Finally, for $\gamma > \gamma_s$, a pair of real inverse eigenvalues leaves the unit circle to slide on the real line while a pair of eigenvalues remains at $+1$. In that case, the stability of the periodic solution is lost. For $\gamma = 0.181$, one of the eigenvalues of modulus around 5.71 is not displayed. To illustrate this loss of stability, we report, in Fig. 9, several time integrations of the system with constraints and impacts for different values of

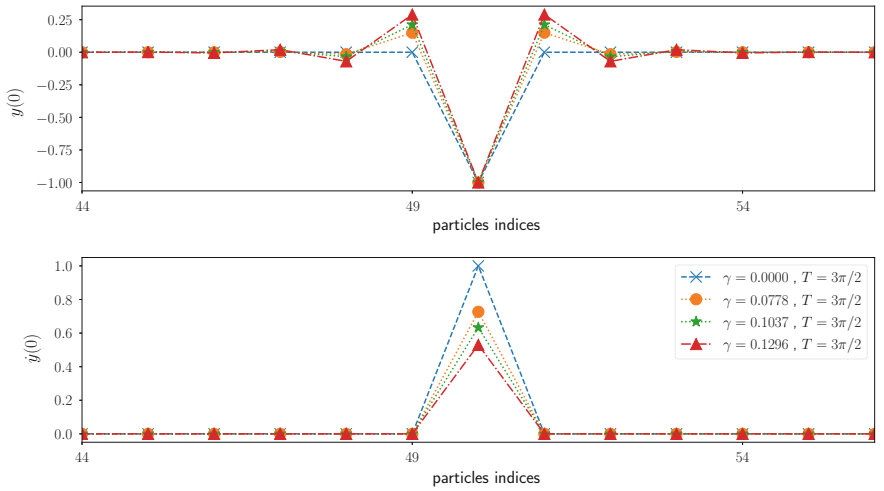

Fig. 7 Site-centered breather with pattern $I_1 = \emptyset$, $I_2 = \{50\}$

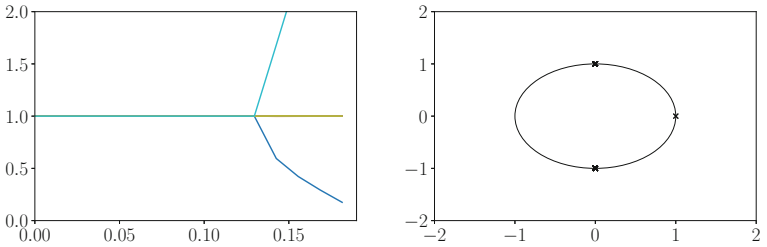

(a) modulus of the eigenvalues $|\lambda_i|$ versus γ

(b) eigenvalues for $\gamma = 0$

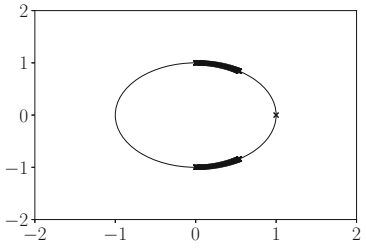

(c) eigenvalues for $\gamma = 0.064$

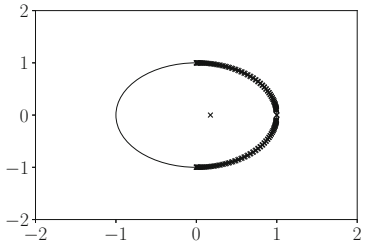

(d) eigenvalues for $\gamma = 0.181$

Fig. 8 Eigenvalues of the monodromy matrix for the site-centered breather with pattern $I_1 = \emptyset$, $I_2 = \{50\}$

γ over the time interval $[0, 25T]$. Although the system is numerically integrated with high accuracy Runge-Kutta schemes in ODEPACK with very tight tolerances (10^{-14}), the periodic solutions for $\gamma = 0.181$ are destabilized.

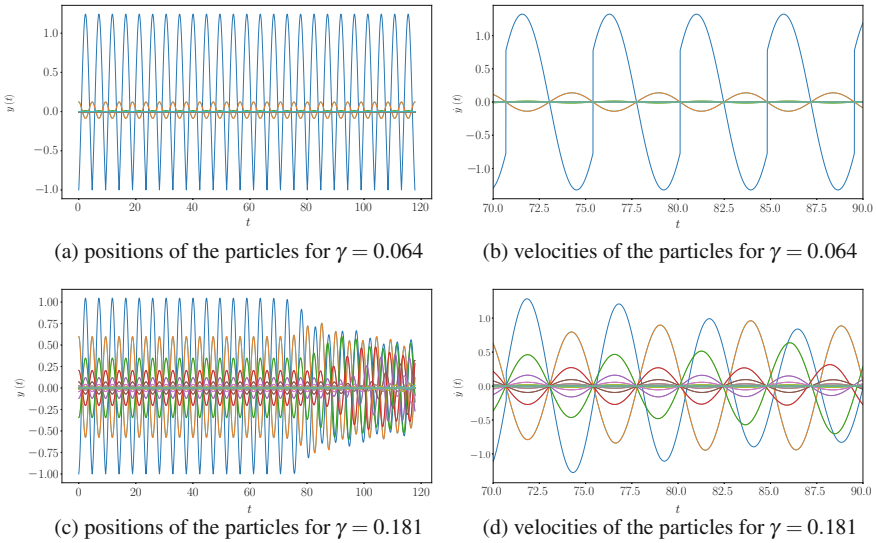

(a) positions of the particles for $\gamma = 0.064$

(b) velocities of the particles for $\gamma = 0.064$

(c) positions of the particles for $\gamma = 0.181$

(d) velocities of the particles for $\gamma = 0.181$

Fig. 9 Time integration of the periodic solutions for the site-centered breather with pattern $I_1 = \emptyset$, $I_2 = \{50\}$

We also perform a continuation of the solution with respect to the period. We start for a value of (γ, T) equal to $(0.15, 3\pi/2)$ and we decrease the period following a solution with a fixed pattern. The numerical solutions are displayed in Fig. 10a. We can observe that a family of site-centered breathers is found with an increasing amplitude of the initial state. For the uncoupled case ($\gamma = 0.0$), we know that the amplitude of the solution goes to infinity when $T \to \pi$. The same phenomenon is observed for a given coupling parameter $\gamma = 0.15$. In Fig. 10b, we plot the maximum amplitude of the position $\|y(0)\|_\infty$ and the velocity $\|\dot{y}(0)\|_\infty$ as a function of T. An asymptotic value of the period clearly appears for which the amplitude of the solution blows up. In this specific case, the asymptotic value of the period is about $0.58(3\pi/2) \approx 2.78$. Let us note that this value is below π.

To conclude this section, an exploration of the viability of the site-centered breathers has been performed for $(\gamma, T) \in [0, 1.1] \times [2, 2\pi]$ and $p = 30$ particles. We select a mesh grid in the plane (γ, T) and solve the boundary value problem for each pair (γ, T). The results are reported in Fig. 11. The light areas correspond to a numerical computation of a periodic solution to (12)–(13) with the satisfaction of the constraint (14) and the pattern $I_1 = \emptyset$, $I_2 = \{15\}$. The red dashed curve is given by the out-of-phase grazing linear mode whose period is related to γ by

$$T(\gamma) = 2\pi\,(1 + 4\gamma)^{-1/2}. \tag{46}$$

As expected with the previous computations, we observe that there exists a large light area bounded above by the relation (46) and corresponding to site-centered

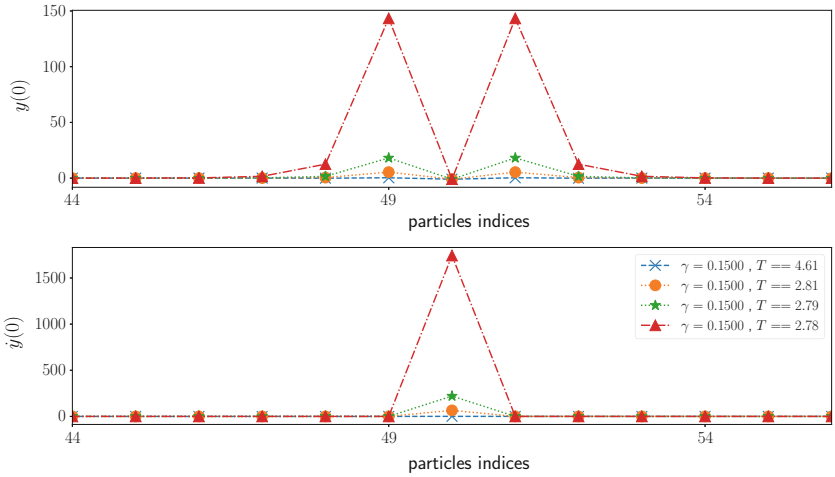

(a) positions and velocities of the particles

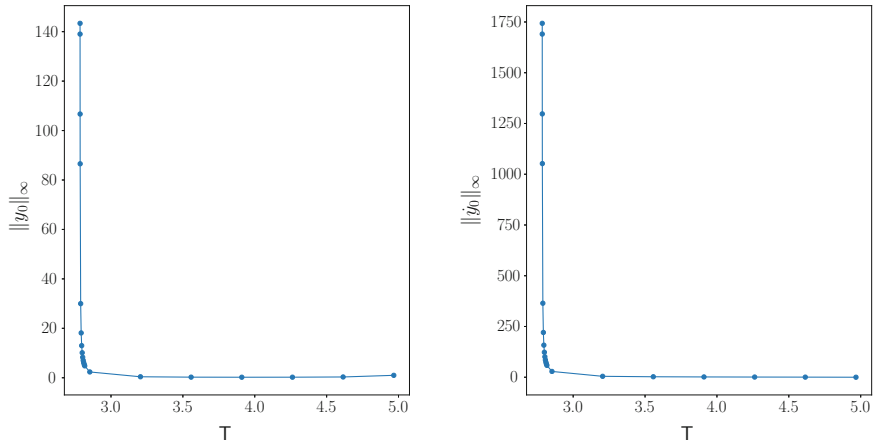

(b) maximum amplitude of the position $\|y(0)\|_\infty$ and the velocity $\|\dot{y}(0)\|_\infty$ as a function of T

Fig. 10 Continuation with a decreasing period of the site-centered breather with pattern $I_1 = \emptyset$, $I_2 = \{50\}$ for $\gamma = 0.15$

breathers. This area is also bounded below by another curve that corresponds to modes whose amplitudes go to infinity, as we have already discussed for a particular value of $\gamma = 0.15$ in Fig. 10. Quite interestingly, other light areas are present above the red curve. To explain these areas, we plot the graphs of the periods with respect to γ for larger wavenumber q given by

$$T_n(\gamma) = 2\pi \left(1 + 4\gamma \sin^2(q/2)\right)^{-1/2}, \text{ with } q = n2\pi/p, \quad n = 1, \ldots, 15. \tag{47}$$

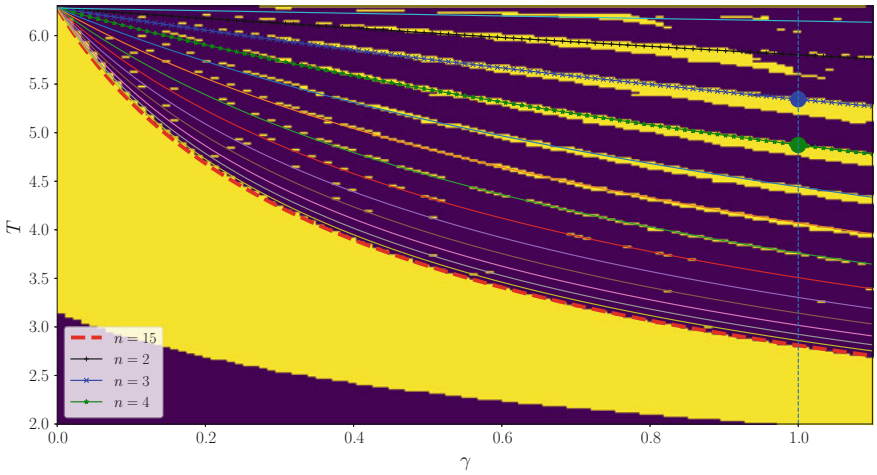

Fig. 11 Continuation of periodic solutions with pattern $I_1 = \emptyset$, $I_2 = \{15\}$ (light areas) for $(\gamma, T) \in [0, 1.1] \times [2, 2\pi]$. Graphs of $T_n(\gamma) = 2\pi \left(1 + 4\gamma \sin^2(q/2)\right)^{-1/2}$, with $q = n2\pi/p$, for $n = 1, \ldots, 15$ and $p = 30$

We can observe the existence of modulated waves near the linear grazing solutions. In order to illustrate the solutions obtained in these areas, we plot, in Fig. 12, the results of two continuations over the period for $\gamma = 1$, $T_3 \approx 5.34$ and $T_4 \approx 4.87$ (large dots in Fig. 11). We can observe that these solutions are not exactly normal nonsmooth modes that emerge from the linear grazing modes, but rather spatial modulations of nonsmooth normal modes. For the computation of what could be called a *nonsmooth normal mode*, we refer to Sect. 3.4. There, other solutions are computed (with long-wavelength near T_1) with preservation of the normal mode pattern at the start of continuation.

3.2 Bond-Centered Breathers

In this section, some bond-centered breathers are computed with two different patterns.

Bond-Centered Breathers With Pattern $I_1 = \{49\}$, $I_2 = \{50\}$

Let us start with the out-of-phase pattern $I_1 = \{49\}$, $I_2 = \{50\}$, illustrated in Fig. 13. We again choose a period equal to $\frac{3\pi}{2}$, and the periodic solution has successfully been computed in the range $[0, \gamma_c]$, with γ_c given by (45). The initial conditions of the periodic solutions are displayed in Fig. 14 for the particle indices in $[40, 60]$. Again, we can observe that the breather is localized over a few particles for small values of the coupling parameter. Once again, the solution reaches the out-of-phase

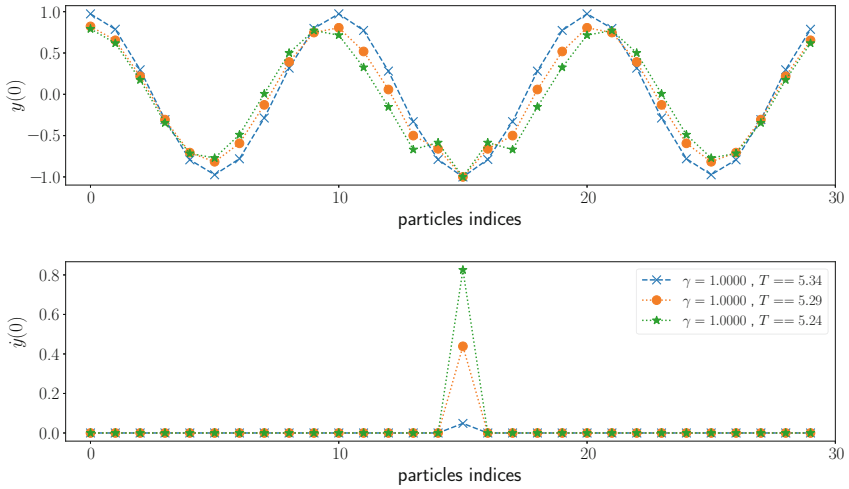

(a) Continuation for the value of the period around $T_3 = 2\pi\left(1+4\gamma\sin^2(3\pi/30)\right)^{-1/2} \approx 5.34$

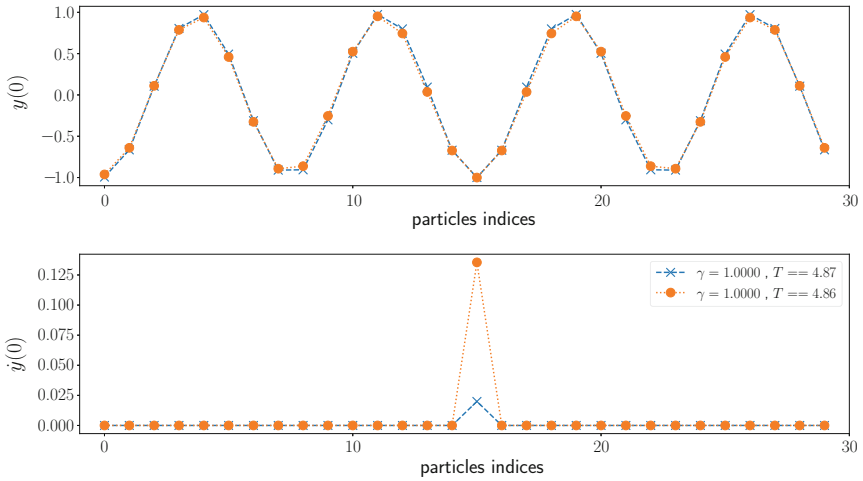

(b) Continuation for the value of the period around $T_4 = 2\pi\left(1+4\gamma\sin^2(4\pi/30)\right)^{-1/2} \approx 4.87$

Fig. 12 Continuation of spatially-modulated nonsmooth normal modes with pattern $I_1 = \emptyset$, $I_2 = \{15\}$ for $\gamma = 1$

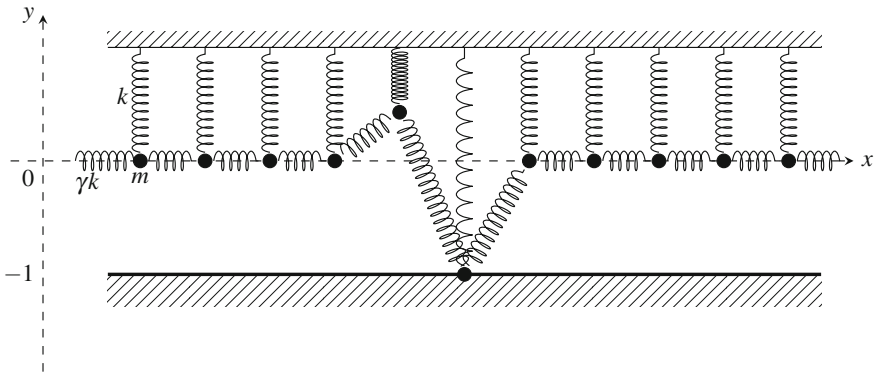

Fig. 13 Mode pattern for the bond-centered breather

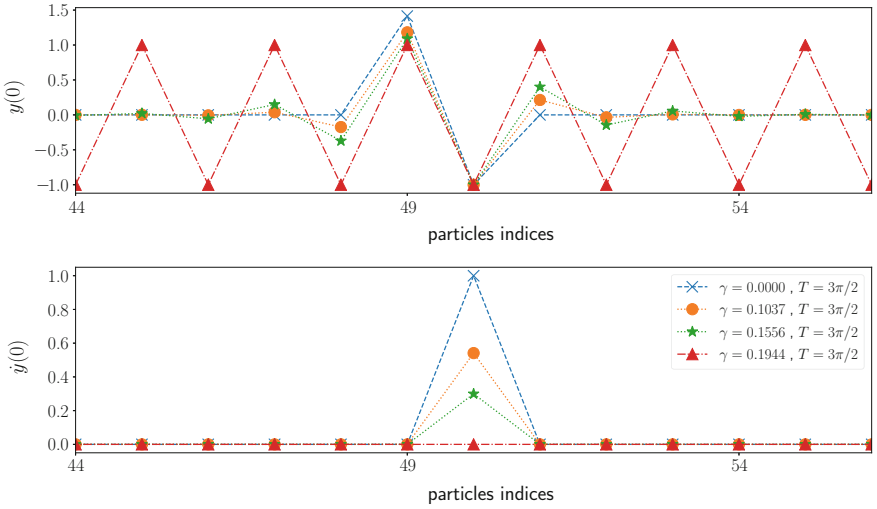

Fig. 14 Bond-centered breather with pattern $I_1 = \{49\}$, $I_2 = \{50\}$

linear grazing mode for $\gamma = \gamma_c$ while the velocity of the central particle decreases at time 0.

In Fig. 15, we depict the eigenvalues of the monodromy matrix. In Fig. 15b, for $\gamma = 0$, we have two pairs of eigenvalues in $+1$. All the other pairs of conjugate eigenvalues are equal to i or $-i$. We observe, in Fig. 15a and b, that for $\gamma > 0$, a pair of real inverse eigenvalues slides from $+1$ on the real line as γ increases, while the other pair remains equal to $+1$. The others pairs of conjugate eigenvalues slide on the unit circle toward the pair of real eigenvalues in $+1$. A collision occurs again at $+1$ for $\gamma = \gamma_s \in [0.142, 0.155]$. Then, a second pair of inverse real eigenvalues slides on the real line. For $\gamma > 0$, the stability of the periodic solutions is lost. We

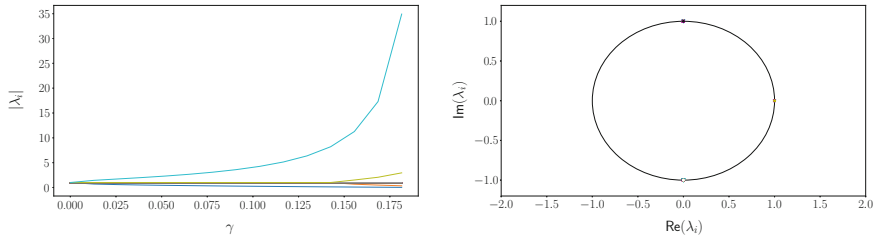

(a) modulus of the eigenvalues $|\lambda_i|$ versus γ

(b) eigenvalues for $\gamma = 0$

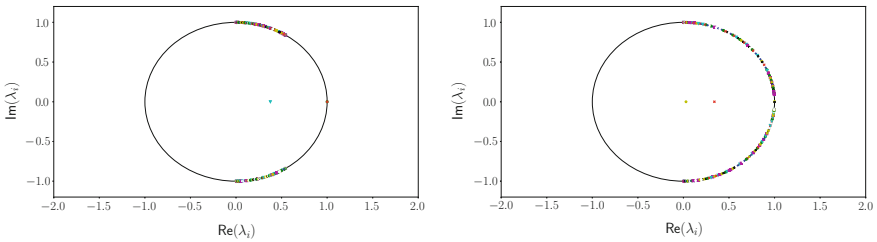

(c) eigenvalues for $\gamma = 0.064$

(d) eigenvalues for $\gamma = 0.181$

Fig. 15 Eigenvalues of the monodromy matrix for the bond-centered breather with pattern $I_1 = \{49\}$, $I_2 = \{50\}$

attempt to illustrate this phenomena with numerical time integration of the periodic solutions over a long time interval $[0, 35T]$ in Fig. 16.

Bond-Centered Breathers With Pattern $I_1 = \emptyset$, $I_2 = \{49, 50\}$

For the pattern $I_1 = \emptyset$, $I_2 = \{49, 50\}$, the solution for the initial conditions is depicted for the whole chain in Fig. 17a and for the particles with indices in [40, 60] in Fig. 17b. The period is again $\frac{3\pi}{2}$, and we succesfully perform a continuation of the solution over $[0, \gamma_c]$ with γ_c given by (45). The main difference with the previous breathers concerns the solution when $\gamma \to \gamma_c$. In this latter case, it seems that we do not converge towards a grazing linear mode. This has to be confirmed with a more accurate study of the critical value of γ.

In Fig. 18, we depict the eigenvalues of the monodromy matrix computed by finite differences. In this case, the closed form formula of the monodromy (44) no longer applies, since we have multiple impacts. Although the approximation of the eigenvalues may contain some numerical errors, we observe a more complicated behavior of the evolution with respect to γ of the eigenvalues. For $\gamma = 0$, two pairs of real eigenvalues are equal to $+1$ and the others are conjugated pairs of eigenvalues equal to i and $-i$. For increasing values of γ, one of the pairs of real eigenvalues starts to slide on the unit circle, respectively towards i and $-i$, while the other pairs of conjugate eigenvalues slide on the unit circle from i and $-i$ towards $+1$. A first collision occurs on the unit circle for $\gamma \in [0.051, 0.064]$ and two pairs of eigenvalues leave the unit circle. Several other collisions of different types occur when we increase the value of γ up to γ_c.

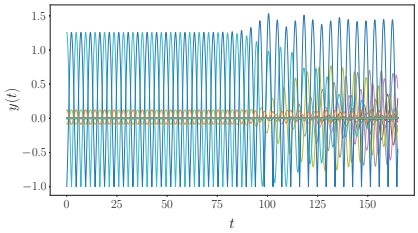

(a) positions of the particles for $\gamma = 0.064$

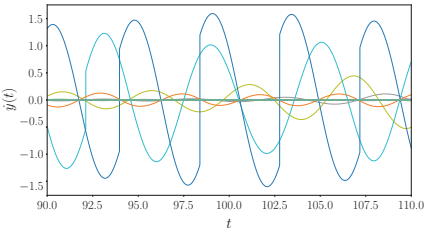

(b) velocities of the particles for $\gamma = 0.064$

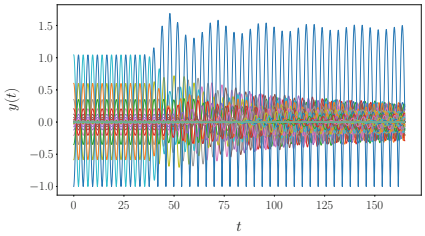

(c) positions of the particles for $\gamma = 0.181$

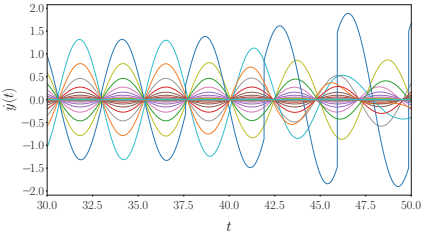

(d) velocities of the particles for $\gamma = 0.181$

Fig. 16 Time integration of the periodic solutions for the bond-centered breather with pattern $I_1 = \{49\}$, $I_2 = \{50\}$

3.3 Multiple Impacting Particles

In this section, we illustrate wave patterns with multiple impacts, where the pattern is either spatially periodic or localized on several particles (multi-site breathers).

Out-of-Phase Mode with Spatial Period Two

We start with the nonsmooth mode of spatial period two described in Sect. 2. The pattern is given by $I_1 = \{2k+1\}_{k=0,\ldots,49}$, $I_2 = \{2k\}_{k=0,\ldots,49}$, which corresponds to the sets of odd and even integers, respectively. In Fig. 19, the initial conditions for the periodic solutions are given for $T = \frac{3\pi}{2}$. For this example, we are able to continue the solution over the range $[0, \gamma_c]$ up to reaching the out-of-phase linear grazing mode. In Fig. 20, the eigenvalues of the monodromy matrix computed by finite differences are depicted. For $\gamma = 0$, all the eigenvalues are equal to $+1$. For $\gamma > 0$, the pairs of inverse real eigenvalues slide on the real line. The periodic solutions are therefore unstable for $\gamma > 0$. This is illustrated in Fig. 21, where long time integration simulations have been performed over the time interval $[0, 35T]$.

Periodic Wave with Spatial Period Six

Another example of nonsmooth spatially periodic standing wave is displayed in Fig. 22. The spatial period is six and the time period is again $\frac{3\pi}{2}$. The mode profiles are depicted for several values of γ in $[0, \gamma_c]$.

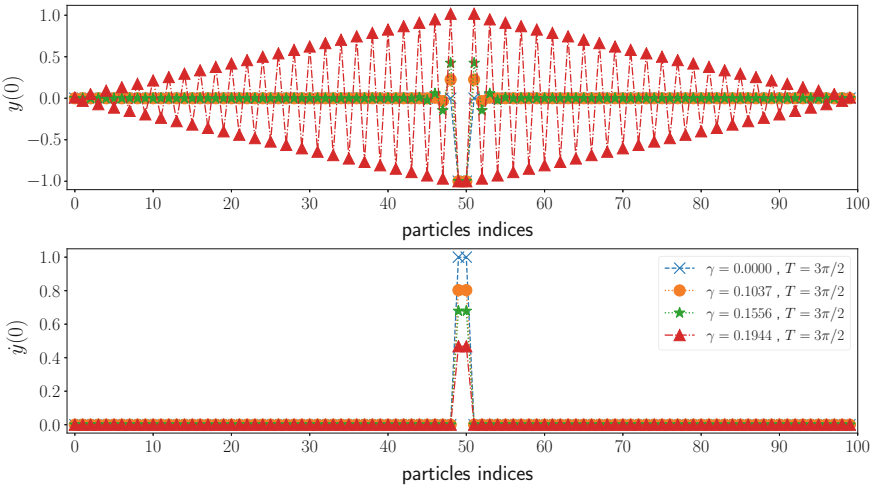

(a) initial positions and velocities of the particles

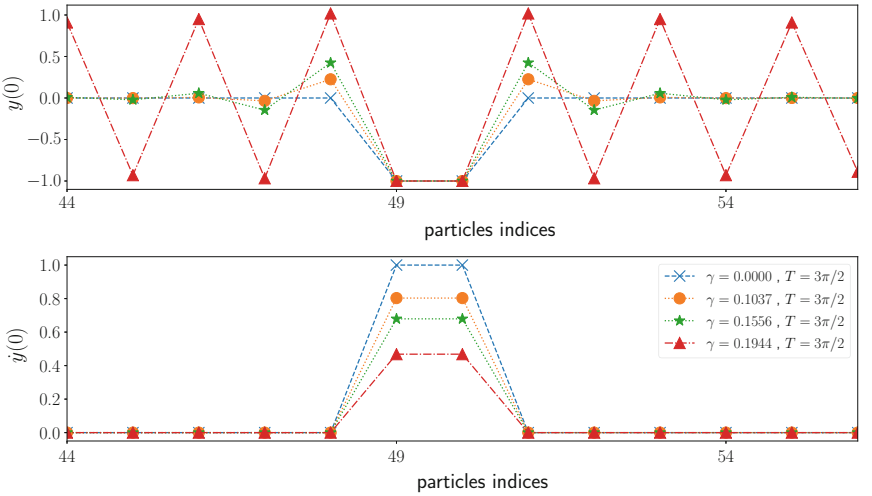

(b) initial positions and velocities of the particles with indices in $[40, 60]$

Fig. 17 Bond-centered breather with pattern $I_1 = \emptyset$, $I_2 = \{49, 50\}$

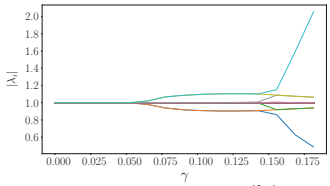

(a) modulus of the eigenvalues $|\lambda_i|$ versus γ

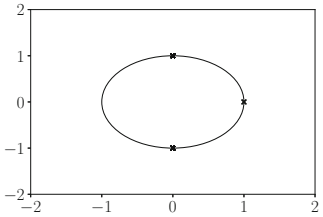

(b) eigenvalues for $\gamma = 0$

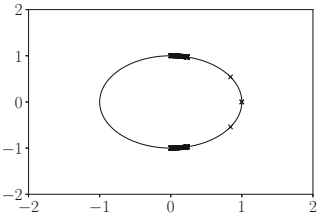

(c) eigenvalues for $\gamma = 0.025$

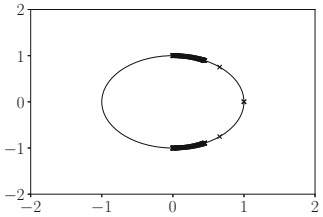

(d) eigenvalues for $\gamma = 0.051$

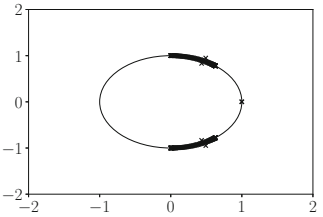

(e) eigenvalues for $\gamma = 0.077$

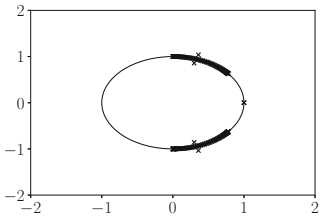

(f) eigenvalues for $\gamma = 0.103$

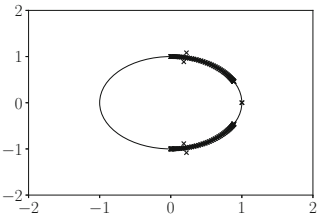

(g) eigenvalues for $\gamma = 0.129$

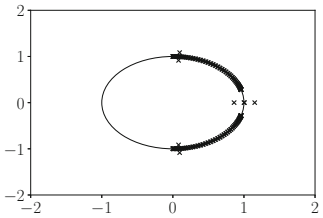

(h) eigenvalues for $\gamma = 0.155$

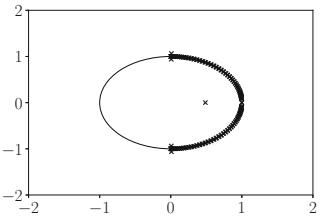

(i) eigenvalues for $\gamma = 0.181$

Fig. 18 Eigenvalues of the monodromy matrix computed by finite differences for the bond-centered breather with pattern $I_1 = \emptyset$, $I_2 = \{49, 50\}$

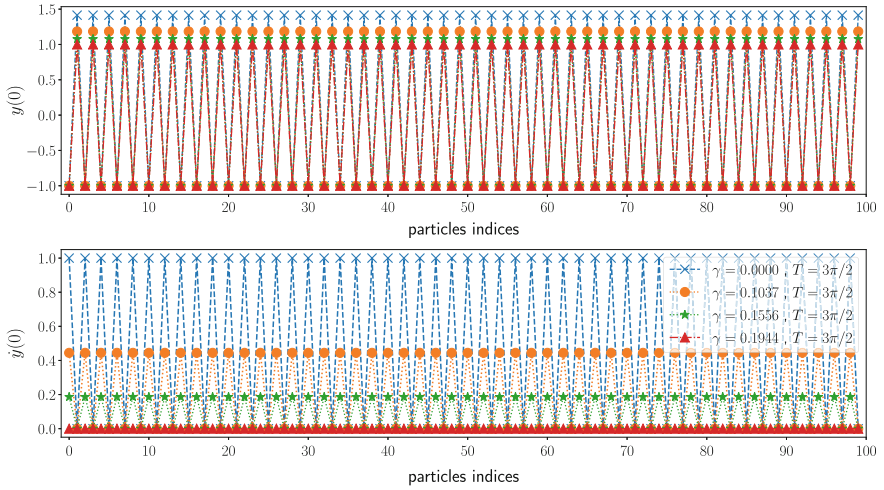

Fig. 19 Out-of-phase mode with pattern $I_1 = \{2k+1\}_{k=0,\ldots,49}$, $I_2 = \{2k\}_{k=0,\ldots,49}$

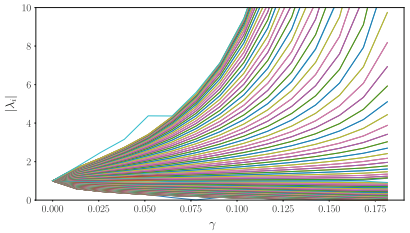

(a) modulus of the eigenvalues $|\lambda_i|$ versus γ

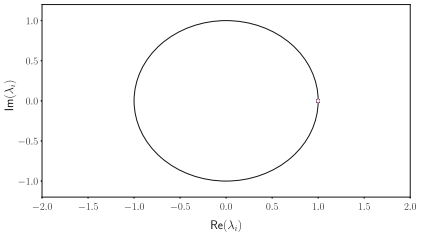

(b) eigenvalues for $\gamma = 0$

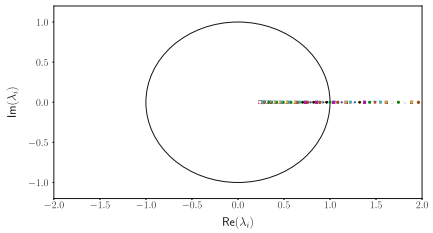

(c) eigenvalues for $\gamma = 0.064$

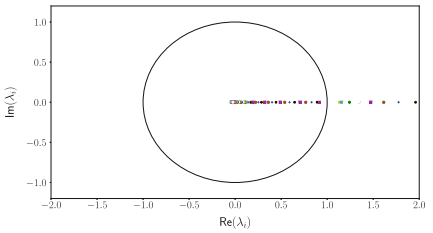

(d) eigenvalues for $\gamma = 0.181$

Fig. 20 Eigenvalues of the monodromy matrix computed by finite differences for the out-of-phase mode with pattern $I_1 = \{2k+1\}_{k=0,\ldots,49}$, $I_2 = \{2k\}_{k=0,\ldots,49}$

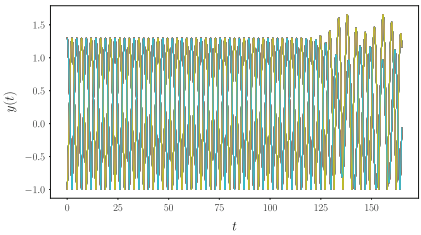

(a) positions of the particles for $\gamma = 0.051$

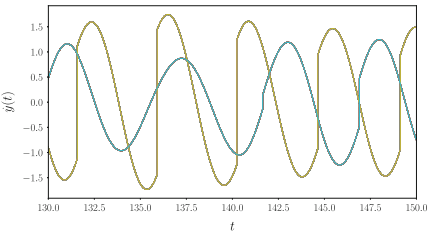

(b) velocities of the particles for $\gamma = 0.051$

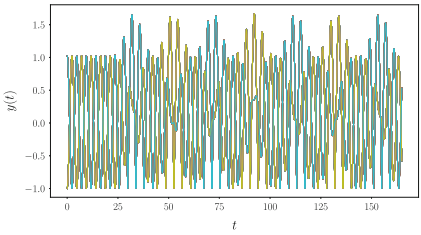

(c) positions of the particles for $\gamma = 0.181$

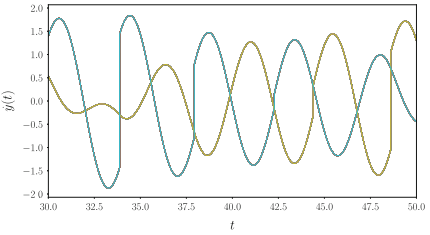

(d) velocities of the particles for $\gamma = 0.181$

Fig. 21 Time integration of the periodic solutions for the out-of-phase mode with pattern $I_1 = \{2k+1\}_{k=0,\ldots,49}$, $I_2 = \{2k\}_{k=0,\ldots,49}$

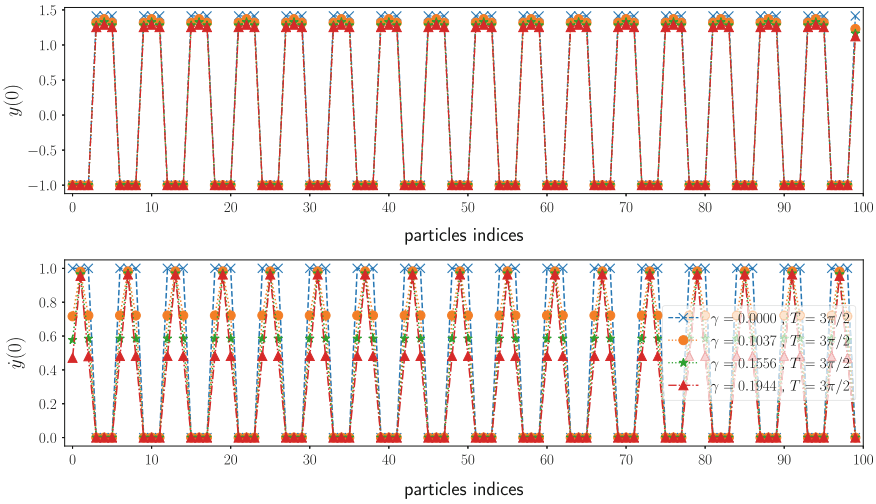

Fig. 22 Periodic wave with pattern of spatial period 6 : $I_1 = \{6k+3, 6k+4, 6k+5\}_{k=0,3,\ldots}$, $I_2 = \{6k, 6k+1, 6k+2\}_{k=0,3,\ldots}$

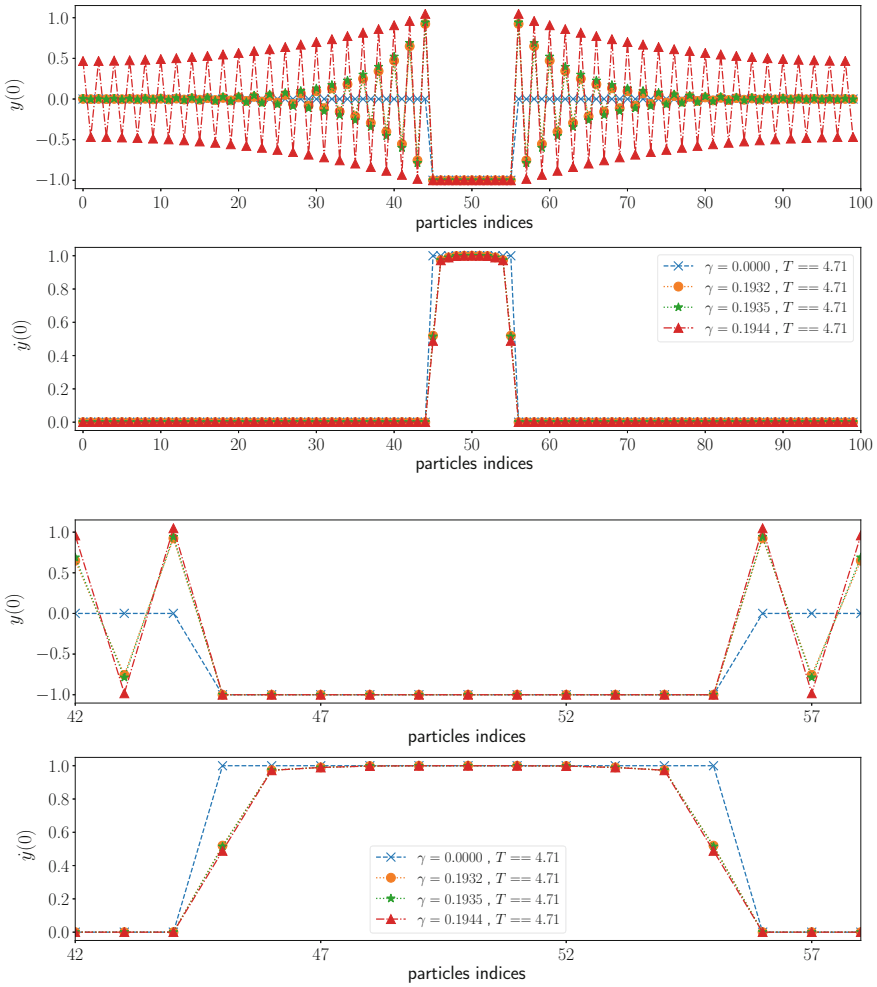

Fig. 23 Multi-site breather with pattern $I_1 = \emptyset$, $I_2 = \{45, \ldots, 55\}$

Multi-site Breather Localized on 10 Particles

In Fig. 23, a multi-site breather with pattern $I_1 = \emptyset$, $I_2 = \{45, \ldots, 55\}$ is displayed for $T = \frac{3\pi}{2}$. For $\gamma \to \gamma_c$, the computation of the solutions is more difficult. The largest value of γ for which a solution is displayed is $0.1944096 < \gamma_c$. We can observe that the particles in I_0 are still not grazing.

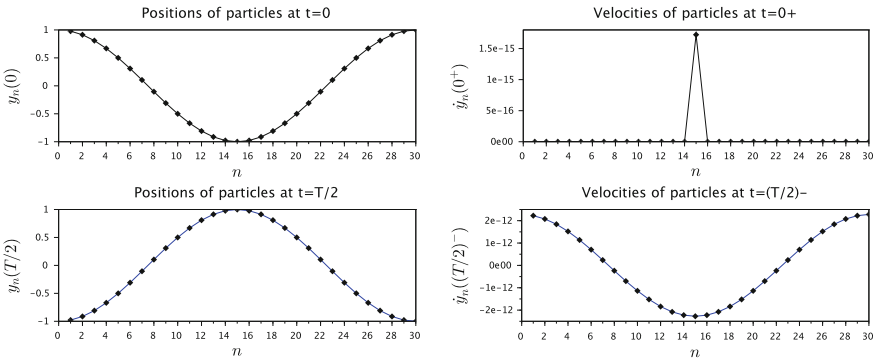

(a) Positions for $T = T_1$ (b) Velocities for $T = T_1$

Fig. 24 Main linear grazing mode for $\gamma = 1$ and $T_1 = 2\pi\ (1 + 4\gamma \sin^2(\pi/30))^{-1/2}$

3.4 Long-Wavelength Modes

We also compute spatially extended long-wavelength modes close to the main linear mode with wavenumber $q = 2\pi/p$, that is depicted in Fig. 24. The period of the linear mode for a given wavenumber q is

$$T_1 = 2\pi\ (1 + 4\gamma \sin^2(q/2))^{-1/2}. \tag{48}$$

Our computations are performed for $\gamma = 1$ and $p = 30$ particles and we get $T_1 \approx 6.150$.

A First Branch of Solutions

We are able to follow a first continuous branch of solutions depicted in Fig. 25 with periods $T \in [\alpha_7\, T_1, \alpha_1\, T_1]$, and $\alpha_1 = 0.99056$ and $\alpha_7 = 0.5035988$. The mode amplitude diverges when $T \to \alpha_7\, T_1^+$, and two particles at $n = 15, 30$ (the antinodes, i.e., the particles that reach maximal height) undergo grazing impacts when $T \to \alpha_1\, T_1^-$. The number of impacting particles decreases from 30 to 10 when T is increased. More precisely, for T in intervals of the form $[\alpha_j\, T_1, \alpha_{j-1}\, T_1]$, we find $4j + 2$ impacting particles with pattern $I_1 = \{1, 2, \ldots, j, p - j, p - j + 1, \ldots, p\}$, $I_2 = \{15 - j, \ldots, 15 + j\}$. We find $\alpha_6 \approx 0.5798, \alpha_5 \approx 0.7641, \alpha_4 \approx 0.92, \alpha_3 \approx 0.9618, \alpha_2 \approx 0.9771$.

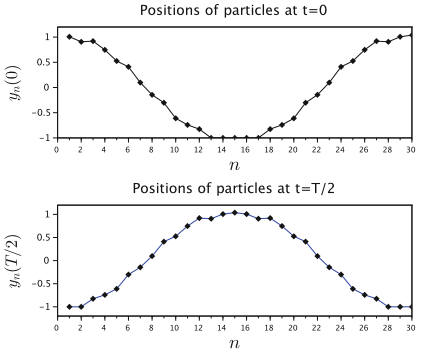

(a) Positions for $T = \alpha_1 T_1$

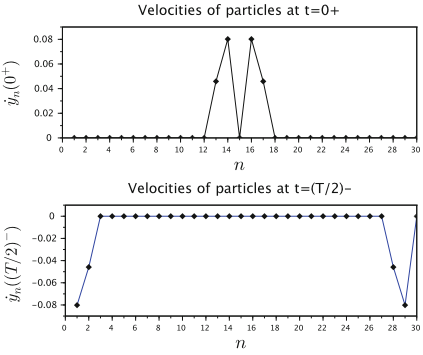

(b) Velocities for $T = \alpha_1 T_1$

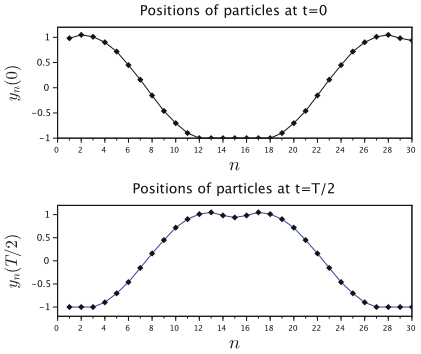

(c) Positions for $T = \alpha_2 T_1$

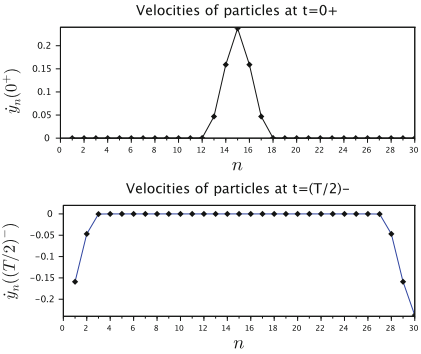

(d) Velocities for $T = \alpha_2 T_1$

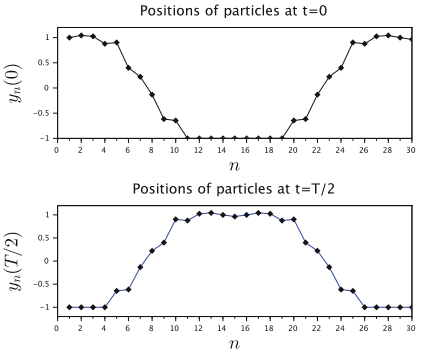

(e) Positions for $T = \alpha_3 T_1$

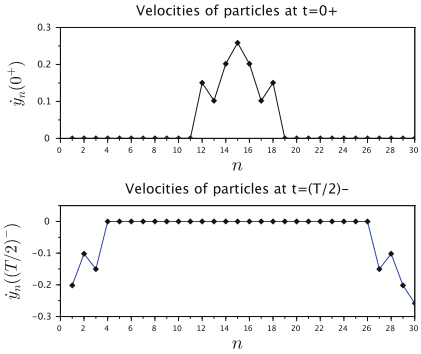

(f) Velocities for $T = \alpha_3 T_1$

Fig. 25 A first branch of long-wavelength normal modes for $\gamma = 1$ and $T_1 = 2\pi \left(1 + 4\gamma \sin^2(\pi/30)\right)^{-1/2}$

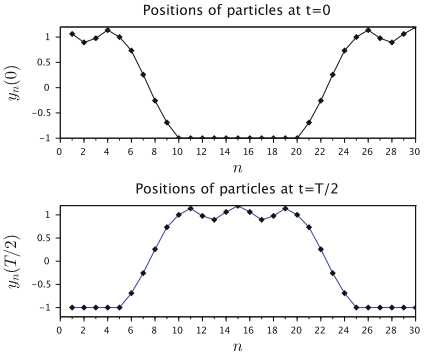

(g) Positions for $T = \alpha_4 T_1$

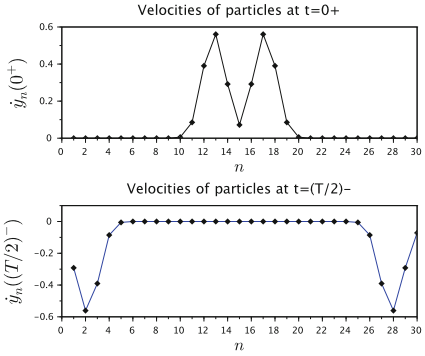

(h) Velocities for $T = \alpha_4 T_1$

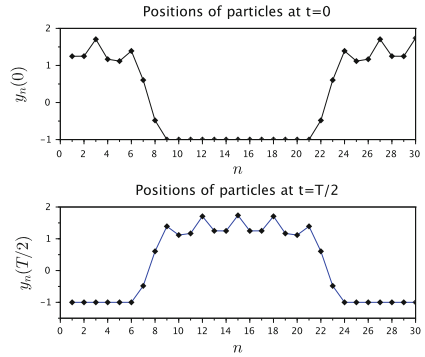

(i) Positions for $T = \alpha_5 T_1$

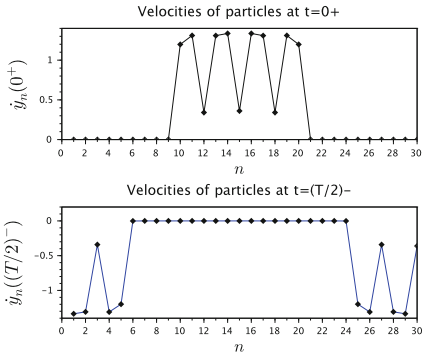

(j) Velocities for $T = \alpha_5 T_1$

Fig. 25 (continued)

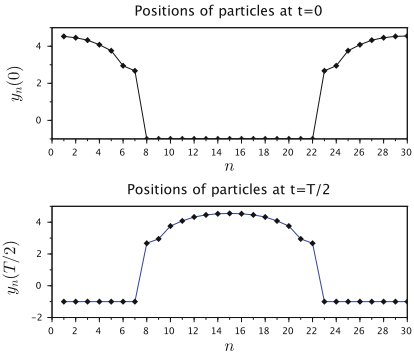

(k) Positions for $T = \alpha_6 T_1$

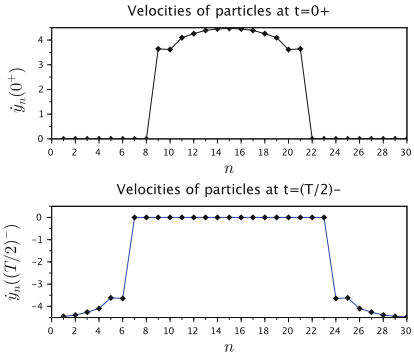

(l) Velocities for $T = \alpha_6 T_1$

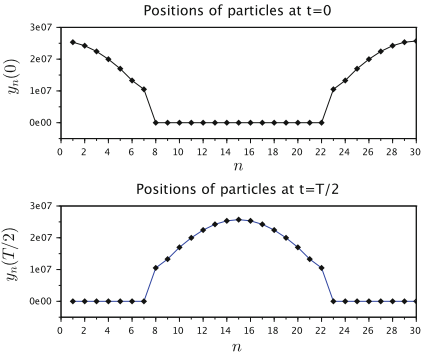

(m) Positions for $T = \alpha_7 T_1$

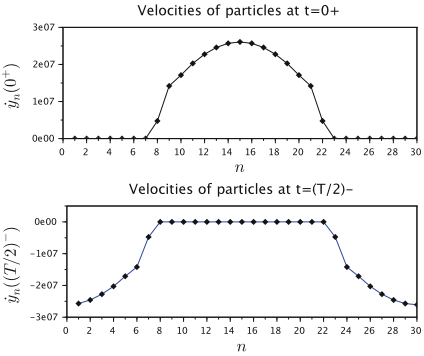

(n) Velocities for $T = \alpha_7 T_1$

Fig. 25 (continued)

A Second Branch of Solutions

We find another branch of solutions whose period $T \in [0.81 \cdot T_1, T_1)$ can approach T_1 arbitrary closely. These solutions emerge from the linear grazing mode when $T \to T_1$. Let us set $T = \alpha\, T_1$ and describe the mode pattern depending on α. We only describe I_2, given that $I_1 = I_2 + 15 (\mathrm{mod}\, 30)$. We have $I_2 = \{\, 15 \,\}$ for $\alpha \in [0.991, 1)$, $I_2 = \{\, 14, 15, 16 \,\}$ for $\alpha \in [0.9825921, 0.99]$, $I_2 = \{\, 12, 14, 15, 16, 18 \,\}$ for $\alpha \in [0.965, 0.9825924]$, $I_2 = \{\, 11, 12, 14, 15, 16, 18, 19 \,\}$ for $\alpha \in [0.85, 0.964]$, $I_2 = \{\, 9, 11, 12, 14, 15, 16, 18, 19, 21 \,\}$ for $\alpha \in [0.836, 0.849]$, and for $\alpha \in [0.81, 0.835]$, we find $I_2 = \{\, 9, 11, 12, 13, 14, 15, 16, 17, 18, 19, 21 \,\}$. Mode profiles are shown in Fig. 26.

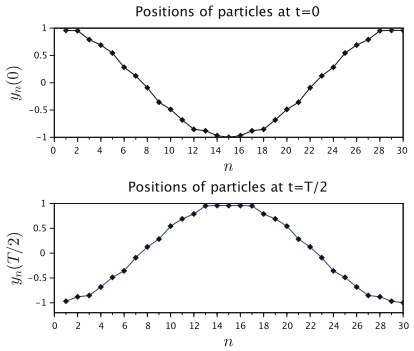

(a) Positions for $T = 0.997T_1$

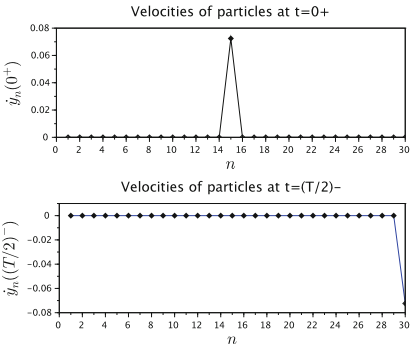

(b) Velocities for $T = 0.997T_1$

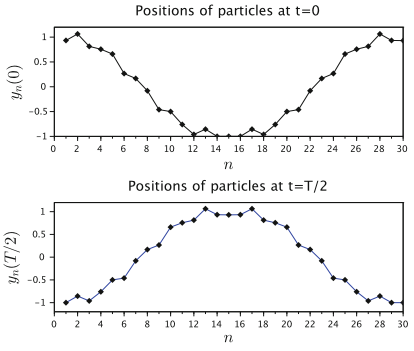

(c) Positions for $T = 0.99T_1$

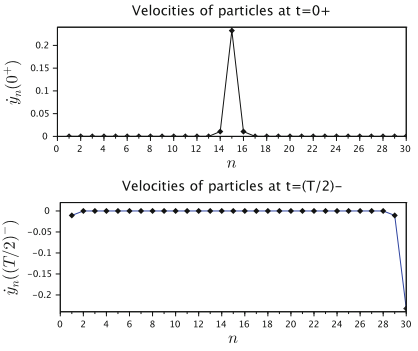

(d) Velocities for $T = 0.99T_1$

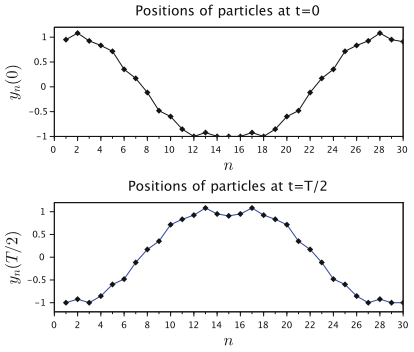

(e) Positions for $T = 0.9825924T_1$

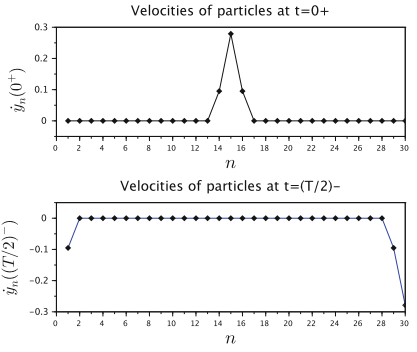

(f) Velocities for $T = 0.9825924T_1$

Fig. 26 A second branch of long-wavelength normal modes for $\gamma = 1$ and $T_1 = 2\pi\,(1 + 4\gamma \sin^2(\pi/30))^{-1/2}$

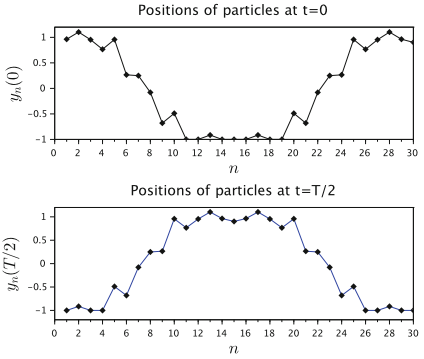

(g) Positions for $T = 0.964T_1$

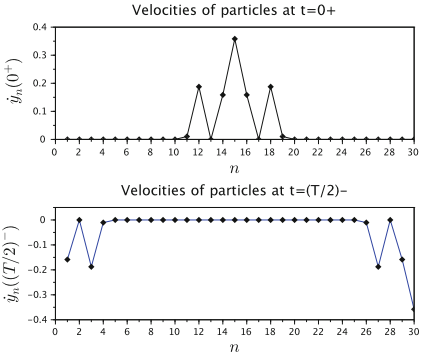

(h) Velocities for $T = 0.964T_1$

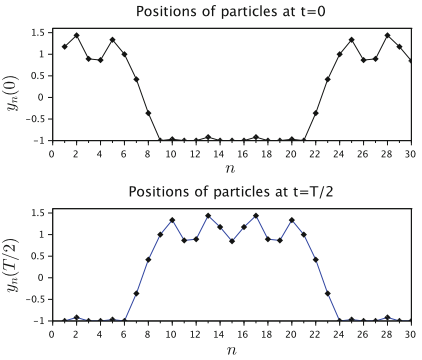

(i) Positions for $T = 0.849T_1$

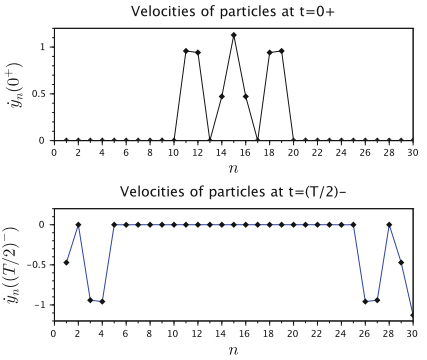

(j) Velocities for $T = 0.849T_1$

Fig. 26 (continued)

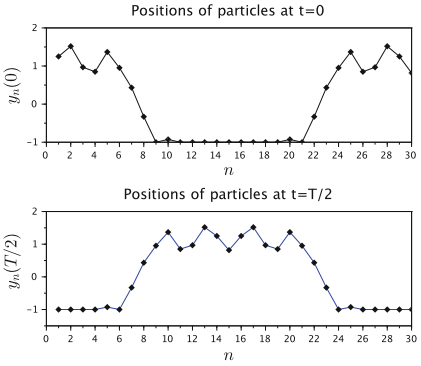

(k) Positions for $T = 0.835T_1$

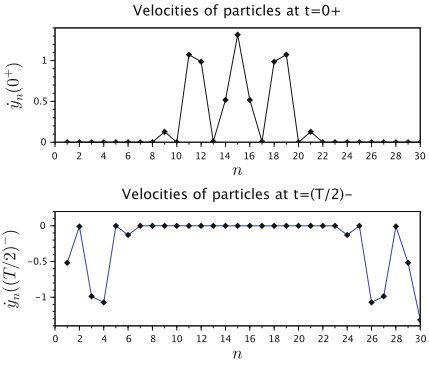

(l) Velocities for $T = 0.835T_1$

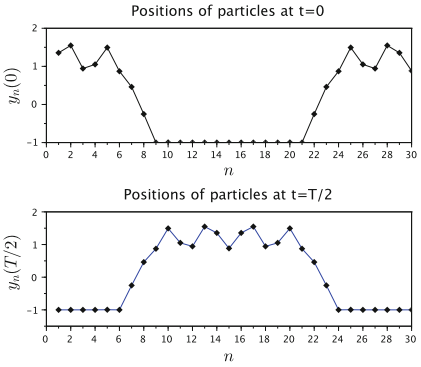

(m) Positions for $T = 0.81T_1$

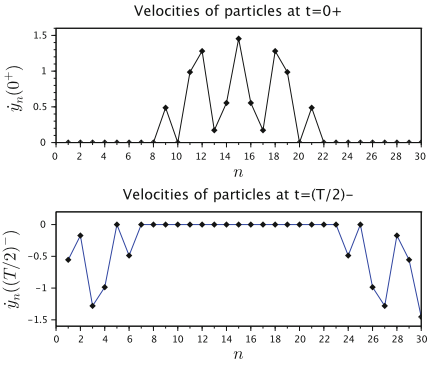

(n) Velocities for $T = 0.81T_1$

Fig. 26 (continued)

4 Discussion

In this work, we have studied the existence and stability of nonsmooth modes (either spatially localized or extended) in a chain of coupled impact oscillators, for rigid impacts without energy dissipation. We have obtained analytical solutions with an arbitrary number of impacting particles at small coupling, and have computed such solutions numerically for larger coupling constants. Different solution branches corresponding to stable or unstable breathers, multibreathers and nonsmooth normal modes have been found.

The computation of periodic solutions based on the above approach is much more effective than numerical continuation of periodic solutions based on stiff compliant models. In the latter case, impacts are described by smooth nonlinear Hertzian type potentials leading to stiff ODE and costly numerical continuation.

Several extensions of this work could be considered. It would be interesting to perform the continuation of periodic solutions while allowing switches in the mode patterns. In addition, the study of more complex types of nonsmooth mode would be of great interest. In particular, one could allow particles to realize several impacts per period [40] or display sticking phases after a grazing contact [27]. The inclusion of dissipative impacts and forcing and the application of the method to more complex finite-element models of continuous impacting systems constitute additional challenging directions.

Acknowledgements The authors are grateful to Oleg Gendelman and Itay Grinberg for all of the stimulating discussions.

References

1. Acary V, Brogliato B (2008) In: Numerical methods for nonsmooth dynamical systems. Applications in mechanics and electronics. Lecture notes in applied and computational mechanics, vol 35. Springer, Berlin
2. Ahn J, Stewart DE (2006) Existence of solutions for a class of impact problems without viscosity. SIAM J Math Anal 38:37–63
3. Astashev VK, Krupenin VL (2001) Experimental investigation of vibrations of strings interacting with point obstacles. Doklady Phys 46:522–525
4. Astashev VK, Krupenin VL (2007) Longitudinal vibrations of a thin rod interacting with an immobile limiter. J Mach Manuf Reliab 36:535–541
5. Babitsky VI (1998) Theory of vibro-impact systems and applications. Foundations of engineering mechanics. Springer, Berlin
6. Babitsky VI, Krupenin VL (2001) Vibration of strongly nonlinear discontinuous systems. Foundations of engineering mechanics. Springer
7. Ballard P (2000) The dynamics of discrete mechanical systems with perfect unilateral constraints. Arch Ration Mech Anal 154:199–274
8. Ballard P (2001) Formulation and well-posedness of the dynamics of rigid-body systems with perfect unilateral constraints. Philos Trans R Soc Lond A 359:2327–2346
9. Cabannes H (1980) Mouvements périodiques d'une corde vibrante en présence d'un obstacle rectiligne. J de Mathématique et de Phys appliquées (ZAMP) 31:473–482
10. Cabannes H (1983) Mouvement d'une corde vibrante en présence d'un obstacle rectiligne fixe. Comptes rendus de l'Académie des sciences Série IIb Mécanique 296:1367–1371
11. Cabannes H (1984) Periodic motions of a string vibrating against a fixed point-mass obstacle: II. Math Methods Appl Sci 6:55–67
12. Cabannes H (1984) Cordes vibrantes avec obstacles. Acta Acust United Acust 55:14–20
13. Cabannes H (1997) Presentation of software for movies of vibrating strings with obstacles. Appl Math Lett 10:79–84
14. Cabannes H, Haraux A (1981) Mouvements presque-périodiques d'une corde vibrante en présence d'un obstacle fixe, rectiligne ou ponctuel. Int J Non-Linear Mech 16:449–458
15. di Bernardo M, Budd CJ, Champneys AR, Kowalczyk P (2008) Piecewise-smooth dynamical systems: theory and applications. Applied mathematical sciences. Springer, Berlin
16. Flach S, Gorbach A (2008) Discrete breathers: advances in theory and applications. Phys Rep 467:1–116
17. Gendelman OV (2013) Exact solutions for discrete breathers in a forced-damped chain. Phys Rev E 87:062911
18. Gendelman OV, Manevitch LI (2008) Discrete breathers in vibroimpact chains: analytic solutions. Phys Rev E 78:026609

19. Grinberg I, Gendelman OV (2016) Localization in finite vibroimpact chains: discrete breathers and multibreathers. Phys Rev E 94:032204
20. Haraux A, Cabannes H (1983) Almost periodic motion of a string vibrating against a straight fixed obstacle. Nonlinear Anal Theory Methods Appl 7:129–141
21. Hindmarsh AC (1983) ODEPACK, a systematized collection of ODE solvers. IMACS Trans Sci Comput 1:55–74
22. http://siconos.gforge.inria.fr/
23. Ibrahim RA (2009) In: Vibro-impact dynamics: modeling, mapping and applications. Lecture notes in applied and computational mechanics, vol 43, Springer, Berlin
24. Krupenin VL (2008) On the analysis of models of strongly nonlinear vibroimpact processes in equipped lattice systems. J Mach Manuf Reliab 37:552–557
25. Krupenin VL (2012) Simulation of vibroshock in two-dimensional systems with inherited properties. J Mach Manuf Reliab 41:361–368
26. Krupenin VL (2017) Vibration of string placed between extended and point limiters. J Mach Manuf Reliab 46:96–104
27. Le Thi H (2017) On some periodic solutions of discrete vibro-impact systems with a unilateral contact condition, PhD thesis, Université Côte d'Azur
28. Lebellego M (2011) Phénomènes ondulatoires dans un modèle discret de faille sismique, PhD thesis, Toulouse University
29. Legrand M, Junca S, Heng S (2017) Nonsmooth modal analysis of a N-degree-of-freedom system undergoing a purely elastic impact law. Commun Nonlinear Sci Numer Simul 45:190–219
30. MacKay RS, Aubry S (1994) Proof of existence of breathers for time-reversible or Hamiltonian networks of weakly coupled oscillators. Nonlinearity 7:1623–1643
31. Manevitch LI, Azeez MAF, Vakakis AF (1999) Exact solutions for a discrete systems undergoing free vibro-impact oscillations. In: Babitsky VI (ed) Dynamics of vibro-impact systems. Springer, Berlin pp 151–158
32. Nqi FZ, Schatzman M (2010) Computation of Lyapunov exponents for dynamical system with impact. Appl Math Sci 4:237–252
33. Perchikov N, Gendelman OV (2017) Dynamics of a discrete breather in a harmonically excited chain with vibro-impact on-site potential, Physica D 292–293: 8–28 (2015). Corrigendum: Physica D 340:26
34. Pilipchuk VN (2001) Impact modes in discrete vibrating systems with rigid barriers. Int J Non-Linear Mech 36:999–1012
35. Schatzman M (1978) A class of nonlinear differential equations of second order in time. Nonlinear Anal 2:355–373
36. Schatzman M (1980) A hyperbolic problem of second order with unilateral constraints: the vibrating string with a concave obstacle. J Math Anal Appl 73:138–191
37. Schatzman M, Bercovier M (1989) Numerical approximation of a wave equation with unilateral constraints. Math Comput 53:55–79
38. Sepulchre J-A, MacKay RS (1997) Localized oscillations in conservative or dissipative networks of weakly coupled autonomous oscillators. Nonlinearity 10:679–713
39. Shiroky IB, Gendelman OV (2016) Discrete breathers in an array of self-excited oscillators: exact solutions and stability. Chaos 26:103112
40. Thorin A, Delezoide P, Legrand M (2017) Nonsmooth modal analysis of piecewise-linear impact oscillators. SIAM J Appl Dyn Syst 16:1710–1747
41. Vakakis AF, Manevitch LI, Mikhlin YV, Pilipchuk VN, Zevin AA (1996). Normal modes and localization in nonlinear systems. Wiley series in nonlinear science
42. Vedenova EG, Manevich LI, Pilipchuk VN (1985) Normal oscillations of a string with concentrated masses on nonlinearly elastic supports. Prikl Mat Mekh 49:203–211
43. Whittlesey EF (1965) Analytic function in Banach spaces. Proc Am Math Soc 16:1077–1083